OPTIMAL DESIGN OF CAPILLARY-WICK FOR HIGH HEAT FLUX THERMAL MANAGEMENT SYSTEM

A Thesis by

Kapot Kallol Tarafder

Bachelor of Science, Bangladesh University of Engineering and Technology, 2012

Submitted to the Department of Mechanical Engineering
and the faculty of the Graduate School of
Wichita State University
in partial fulfillment of
the requirements for the degree of
Master of Science

May 2015

Optimal Design of Capillary-Wick for High Heat Flux Thermal Management System

The following faculty members have examined the final copy of this thesis for form and content, and recommend that it be accepted in partial fulfillment of the requirement for the degree of Master of Science with a major in Mechanical Engineering

Dr. Gisuk Hwang, Committee Chair

Dr. T.S. Ravigururajan, Committee Member

Dr. Vis Madhavan, Committee Member

DEDICATION

I dedicate this work to my Mom, Dad, Pramiti and Prangan.

ACKNOWLEDGMENTS

I thank Department of Mechanical Engineering for supporting me financially and with lab facilities for this study. Special thanks goes to my adviser Dr. Gi-Suk Hwang. It couldn't be any better without him. My heartfelt gratitude to committee members: Dr. T.S. Ravigururajan and Dr. Vis Madhavan. I thank my wife, sister and her family for supporting me through all my struggles. I thank little Prio Prangan for keeping me happy all the time. Most of all I thank my mom who has kept my paralyzed and clinically dead dad alive for more than 6 months.

ABSTRACT

A thermal management system for high heat flux is in great demand as the device sizes become smaller. A failure of the optimal thermal management leads to poor performance, large degradation, and/or complete system breakdown. The optimal thermal management system requires both a low thermal resistance [order of 0.01 K/(W/cm^2)] and high heat flux cooling capability [order of 1 kW/cm^2]. A kinetics of a phase change, i.e., liquid-vapor, provides a good potential to remove high heat flux in evaporators due to a significant latent heat. However, the challenges are the limited liquid supply to the high heat flux surface due to the viscous-capillary limit and a large thermal resistance due to low effective thermal conductivity of the evaporator wick. Here, the optimal evaporator wick for the enhanced liquid supply system is studied using the monolayer and liquid artery wick, to simultaneously reduce the thermal resistance and enhance the heat flux. An innovative liquid artery (thick) wick with monolayer (thin) wick has been demonstrated previously, $q_{CHF} \sim 600$ W/cm^2 with $A_h R_{k,e} < 0.05$ K/(W/cm^2), where the monolayer wick limits the liquid supply to the heated surface and heat transport. Further improvements require the optimal designs of the monolayer wick for desired permeability, porosity, saturation, and capillary meniscus. Geometric optimizations are performed using both the thermal equilibrium and non-equilibrium models including developed close form solutions. For 60 μm particle with the distance between particles 1.12 times the particle diameter, q_{CHF} is obtained around 87 to 90 degree of the angle to the liquid contact, leading to the $q_{CHF} \sim 1$ kW/cm^2. The capillary meniscus recess is also discussed as the liquid morphologies of the monolayer wick drastically change near the particle neck. The effects of the particle size and distance among the particles on the heat flux and thermal resistance are also discussed.

TABLE OF CONTENTS

TABLE OF CONTENTS (continued)

LIST OF TABLES

Table Page

LIST OF FIGURES

Figure Page

LIST OF FIGURES (continued)

LIST OF FIGURES (continued)

Figure Page

LIST OF ABBREVIATIONS AND ACRONYMS

Parameters	Description
A	Area (m^2)
D	Diameter (m)
P	Pressure
V	Volume
K	Permeability (m^2)
L	Distance between adjacent particles (m)
Δh_{lg}	Enthalpy of evaporation (J/kg)
K	Thermal conductivity (W/m-K)
R	Radius (m)
T	Temperature (K)
Greek Symbols	
ε	Porosity
δ_w	Liquid thickness (m)
ρ	Density (kg/m^3)
σ	Surface tension (N/m)
θ	Angle to the liquid contact
Subscript	
a	Artery
c	Capillary
e	Evaporator
f	Fluid
h	Heater
l	Liquid
m	Monolayer
p	Particle
w	Wick
r	Relative

1. INTRODUCTION

Wick thickness modulation assists axial capillary liquid flow, while limiting the increase in the wick superheat. Thicker wick provides low resistance for deporting condensed working fluid from condenser to evaporator while increasing the resistance for heat flow. Modulation of wick structure is widely used in case of microgravity heat pipe. The optimal wick modulation [3] has been validated numerically by Hwang et al. for the circular and flat heat pipes in closed form expressions for the viscous-flow regime for low permeability. This module presented that the maximum enhancement of heat flux is limited by the pipe inner radius, the wick effective thermal conductivity and the prescribed wick superheat limit. Hwang et al. showed that plain heat pipe has highest heat transfer capability but lowest working fluid transport capability. To increase the liquid transport capability wick structure is introduced but if the thickness of the wick is high enough then heat transfer ability is greatly hindered. Here comes the optimization process when the wick thickness plays such a critical role. Then to obtain optimized structure, both thin and thick layers have been introduced to the same structure. This study yielded better result. Modulation of the thick column came into action at this point and the thick columns have been redesigned from squire structure to triangular shapes. Compactness of electronic devices encourages to obtain even higher heat flux. Min et al. along with Hwang et al. presented multi artery heat pipe spreader (MAHPS) [4], MAHPS experiment [3] and MAHPS lateral liquid supply [5] systems to obtain more heat transfer capability. The previous study allows for the heat flux around 500 W/cm^2. Here comes the urge to conduct research on the wick structure to make it more efficient by using monolayer structure with periodic thick columns. To design the monolayer wick structure, parameters i.e. radius of curvature, liquid thickness, permeability, porosity and saturation are taken into account in this current study. High heat flux cooling systems often utilize the two-phase (liquid-gas) latent heat due to a passive, reliable, inexpensive operation. These systems require coolant delivery system to the

heated surface, and liquid permeable structures, i.e. wick, are employed to achieve both the coolant evaporation and delivery. The evaporated coolant in the evaporator delivers heat to the condenser and the condensed coolant returns through wicks to the evaporator via capillary-driven flow. A typical maximum heat transfer rate is determined by the capillary-viscous limit (dry-out).

In previous studies, liquid thickness, radius of curvature for different structures has been studied [3,10,11]. Different permeability model along with saturation is not been studied earlier. The main challenge of this study was to develop equation for saturation for the monolayer wick, which has not been studied so far. Other challenges were to verify the previous standard equations for radius of curvature and liquid thickness, which have been redefined geometrically in this study.

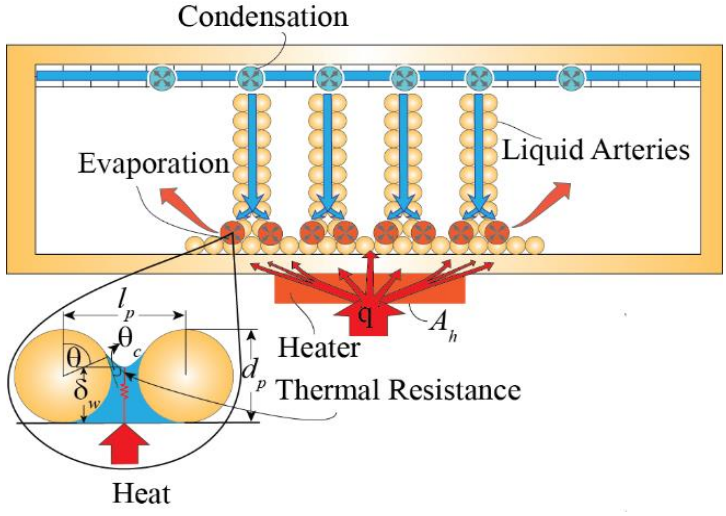

Figure 1 Monolayer porous structure with liquid artery. The evaporation and condensation sites and liquid and vapor pathways are also shown. The capillary meniscus between two particles is also shown.

The thermal resistance that hinders the heat transfer is also a vital concern to get high heat flux so, the size of the particle used to make the monolayer porous structure and the distance between two adjacent particles is also critical for this study. The maximum heat flux is primarily limited by the liquid chocking (dry-out) to the evaporator, while the minimum

thermal resistance is limited by the evaporator wick thickness and effective thermal conductivity of the wicks. Thus, optimal wick design requires both the large liquid supply and the small resistance. Hwang et al. (2007) [9] showed that using a modulated heat pipe without curvature effect can be applied to arrive at eh optimal wick structure design where pipe curvature affects the liquid flow cross-sectional area as well as wick thermal resistance. Strategic liquid supply and vapor escape through high permeable wicks and a large evaporation area has been previously achieved using bi-porous wicks [1, 2] and multi-liquid-artery wick [3-5] structures. The dominant fluid and heat transfer are related to the thin wick of these structures, and to improve the critical heat flux, the examination of optimal thin wick structures is crucial. From these previous studies, it can be inferred that, monolayer porous structure with liquid columns or artery has never been studied closely. From the urge of getting high heat flux in a heat pipe, in this study monolayer porous structure is thus given highest priority. In this study, the optimal design of the monolayer porous structure is studied in great details, such as porosity, capillary meniscus, permeability and liquid saturation. The extensive parametric studies are shown as functions of liquid saturation (effective permeability), porosity (particle density), and particle size.

Our approach for this study was to find the critical value of capillary pressure difference first to ensure that the system does not dry-out. Then mass flow rate is found using critical value of pressure difference. Mass flow rate yields heat flux and finally from heat flux we can calculate the temperature difference between evaporator and condenser. Against different value of θ (angle to the liquid contact), radius of curvature (r_c), liquid thickness (δ), Saturation (S) are plotted to find out the maximum heat flux q(W/cm^2). In this study water is taken as the working fluid as water has very high liquid gas latent heat. As the microporous structure plays a vital role in the mechanism of heat pipe to increase the heat flux, close study of the microporous wick is important. Here, the monolayer wick is designed to examine the critical design

parameters to obtain the knowledge about how the heat flux increases depending on the changes in the design parameters i.e. liquid thickness, radius of curvature of the working fluid between two particles, permeability, porosity and saturation.

1.1 Previous Study

The study that started with Perkin's tube by the patent of A.M. Perkins and J. Perkins in the mid-1800s, came in the light once again by the patent of Gaugler in 1944 as a lightweight passive heat transfer device [14]. After being dormant for about two decades more, with the essence of high heat flux heat transfer device for space program, the idea of heat pipe was patented by Wyatt in 1963 which was suggested by Trefethen in 1962 [15]. Although the term 'heat pipe' was first mentioned by Grover et al. in 1964 to describe a 'synergistic engineering structure, which is equivalent to a material having a thermal conductivity greatly exceeding that of any known metal' [6]. With the development of science and space applications as well as for electronic cooling, which shout high heat flux for more efficient applications, the need for developing heat pipe with more high heat flux was an obvious need to study. To increase the working fluid transport from condenser to evaporator different wick structures influences were patented by Anthony C. Del Bagno, Richard R. Giordano,Frederick Rose in 1984[6]. Later on to achieve high heat flux capability and heat transfer coefficient, thermally driven pulsating two-phase flow [6] is utilized. In this study Zuo, Z.J.; North, M.T.; Wert, K.L found the Critical Heat Flux (CHF) around 250 W/cm^2. By strategic liquid supply and vapor escape through high permeable wicks and a large evaporation area, bi-porous wicks [1,2] and multi artery wick [4] structures have been studied earlier. Multi artery heat pipe study is been extended to the experiment [3] to ensure high heat flux. Multi artery heat pipe spreader: lateral liquid supply [5] is also experimented to increase the critical heat flux.

1.2 Motivation

Heat pipe consists of three basic parts such as

I. Evaporator

II. Condenser and

III. Adiabatic portion.

Evaporator section is the part where heat gets into the heat pipe. Evaporator surface, made up with monolayer copper particles allow the working fluid, water in this case, to evaporate. The goal of this study is to obtain high heat flux and low thermal resistance to ensure that this evaporator portion can lose the heat as fast as possible to ensure faster cooling. The condenser part is the farthest section of heat pipe from evaporator, which caters the environment where the working fluid can be condensed. Water vapor generated from the evaporator section travels through the adiabatic portion to reach the condenser portion. In the adiabatic portion, porous structure is used to ensure the working fluid return path, which increases the resistance to heat transfer. Besides, if the capillary pressure difference is not maintained to a limit, dry-out can occur which might lead the heat pipe to failure. In previous studies, as mentioned earlier, porous wick structure modulation has been studied but optimization of the porous structure in order to improve the liquid transport from the condenser to evaporator after being cooled in the condenser portion might lead towards higher heat flux and lower thermal resistance. Thus, designing the monolayer porous structure, optimization of the affecting criteria will be done, which is the motivation of this study.

1.3 Technical Challenges

In traditional heat pipes, wick structure is typically uniformly thick different, and in turn this leads to the limited heat flux and high thermal resistance.

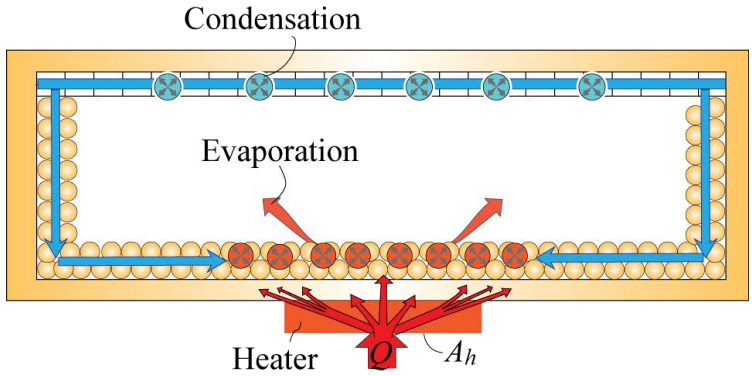

Figure 2 Traditional heat pipe cross section.

In this study, we implement liquid arteries in order to improve fluid transport capability. Although we know that inclusion of liquid artery will result in the decrease in heat flux.

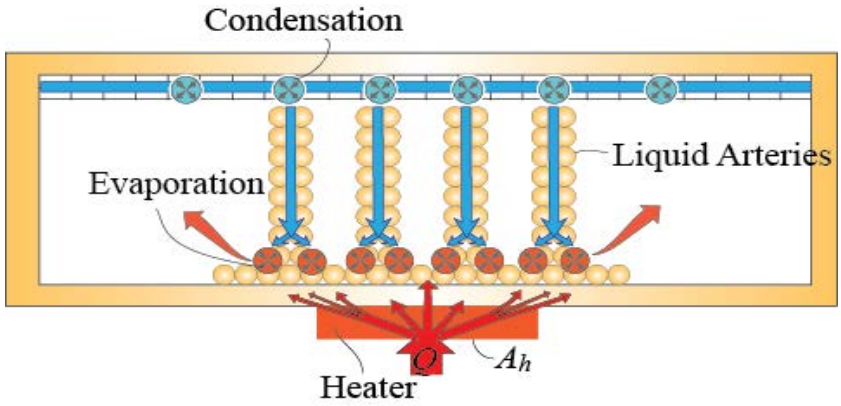

Figure 3 Wick structure with liquid artery.

So the key challenges of our study are:

- Thermal resistance is high
- Liquid transport capability is low

1.4 Research Objective

The main objective of the study is to decrease thermal resistance and increase liquid transport capability. Firstly, close form solutions for the monolayer wick are derived to examine the

liquid morphologies how the parameters are related to the liquid supply and thermal resistance. Secondly, the geometries of the monolayer wick including particle diameter and distance between two adjacent particles are examined aiming at the optimal monolayer wick design.

1.5 Approaches

In micro pore there are two materials copper as solid and water as working fluid. These two materials can be considered as combined material where a single effective thermal conductivity would be considered for both. These two materials can be considered separately where the thermal conductivities are different and temperatures are different as well. So, in this study two approaches are taken for study:

- Thermal Equilibrium Approach
- Thermal Non Equilibrium Approach

2. THERMAL EQUILIBRIUM MODEL

2.1 Model Validation

For developing the basic knowledge and to understand the research goal, gathering all the information from previous studies, first thermal calculation is done along a single liquid artery. Not only thermal study is important but also the flow distribution is important to learn so in the second stage, capillary pressure calculation is done along the same single liquid artery. When temperature and pressure profiles are known, Critical Heat Flux analytical calculation procedure is done using prevailing equations and values from previous studies. At the final stage of the fundamental study diameter and distance between particles are changed to observe how the heat flux changes against temperature difference. When all the fundamental studies will be done, formulations for design parameters are derived using proposed geometry and

then again Critical Heat Flux and particle distance and diameter change effect is calculated again.

2.1.1 Temperature Distribution for Single Column

A single column is studied first for finding the temperature distribution along the column. Figure 4 represents the thermal network for a single column. Five nodes are taken here thus four thermal resistances hinder the heat transfer from the evaporator to the condenser. First thermal resistance is assumed between heater and evaporator surface. Second thermal resistance is considered as the thermal resistance on the evaporator surface before evaporation of the working fluid. As phase change occurs, the vapor temperatures at the evaporation site and at the condensation site are considered as being the same. Third thermal resistance expresses the phase change phenomena and the fourth one represents the resistance on the condenser.

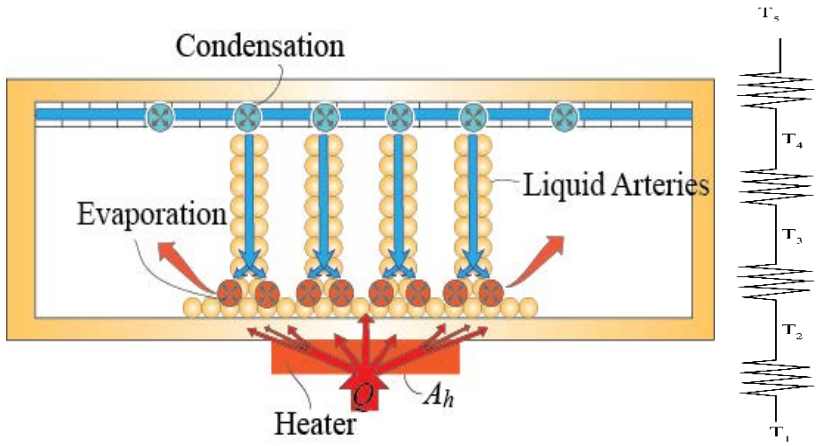

Figure 4 Equilvalant thermal network model

For energy balance, amount of heat transferred through each point in the thermal network, is equal.

$$Q_{1-2} = Q_{2-3} = Q_{3-4} = Q_{4-5}$$

$$Q_{3-4} = Q_{4-5} \quad Q_{2-3} = Q_{3-4} \quad Q_{1-2} = Q_{2-3}$$

$$\Rightarrow \frac{T_3 - T_4}{\frac{L_{he}}{KA}} = \frac{T_4 - T_5}{\frac{L_{hc}}{KA}} \quad \Rightarrow \frac{T_2 - T_3}{\frac{L_{he}}{KA}} = \frac{T_3 - T_4}{\frac{L_{he}}{KA}} \quad \Rightarrow \frac{T_1 - T_2}{\frac{L_h}{K_{cu} A_{cu}}} = \frac{T_2 - T_3}{\frac{L_{he}}{KA}}$$

Table 1 Heat Flux q (W/cm^2) and Temperature Difference ΔT (K) at every node

q(W/ cm^2)	Temperature Difference ΔT
26.4581	5
52.9161	10
79.3742	15
105.8323	20

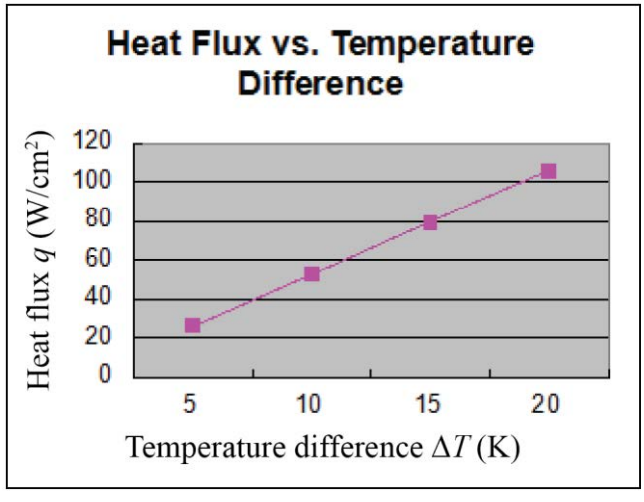

Figure 5 Heat flux q (W/cm^2) as a function of the wick superheat ΔT (K)

2.1.2 Pressure Calculation for Single Column

For calculating pressure at different nodes of a single column of a heat pipe, different nodes are taken into account like the way it was chosen for thermal network. First point of the pressure network is considered on the evaporator surface, second at the bottom of the liquid artery, where the liquid column touches the evaporator surface, third point is taken at the point of column where the liquid artery touches the condenser and the final and fourth point is taken on condenser surface. Considering the mass flow pattern, it is assumed that the amount of working fluid being evaporated from the surface of the evaporator is equal to the amount of working fluid being condensed on the condenser surface.

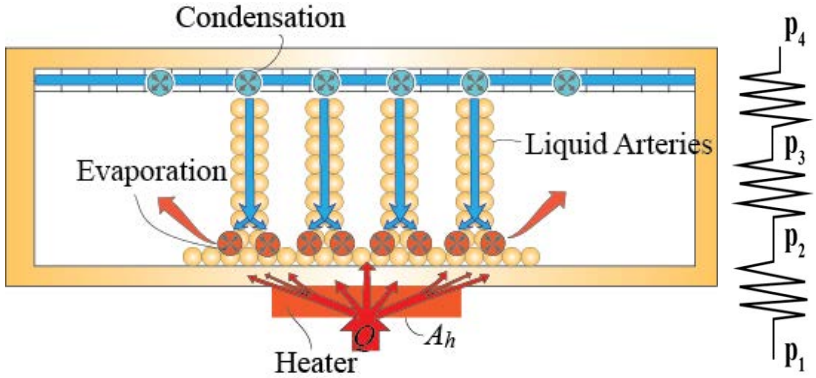

Figure 6 Equivalent flow network model

$\Delta P = \frac{\mu_l l}{K} < v >= \frac{\mu_l l}{K}\frac{\dot{m}}{\rho A}$; So, $\dot{m} = \frac{\Delta p}{R}$ when $R = \frac{\mu_l l}{\rho A K}$

$So, \dot{m} = \frac{P_4 - P_3}{R_3} = \frac{P_3 - P_2}{R_2} = \frac{P_2 - P_1}{R_1} = \frac{Q}{\Delta h_{lg}}$ yields P_1= 89.63 kPa, P_2=92.29 kPa, P_3=101.32 kPa, P_4= 101.33 KPa

Limiting Criterion: $p_4 - p_1 \le \frac{2\sigma}{r_c} = 11.702\,\text{kPa}$

When the input heat is increased beyond the dry-out threshold, nucleate boiling may occur in the wick structure and bubbles may become trapped in the wick. The vapor increases the resistance to the liquid flow, resulting premature evaporator dry-out.

Maximum heat flux is 31.06 W/cm^2.

Maximum temperature difference can be $\Delta T_{\max} = 6^o C$

2.1.3 Critical Heat Flux: Analytical Solution

$q_{CHF} = \frac{Q}{A_h} = \frac{2\sigma \cos\theta_c}{r_c} \frac{k_r \times \rho \times A \times \Delta h_{\lg}}{\mu \times L \times A_h}$; here, r_c=22.23μm, δ_w=42.54μm, $k_r = k$,

q=499.45W/cm^2 and ΔT=84.69 ^{o}C

2.2 Observation by changing different parameters

Before going for the actual study it was necessary to build up knowledge how the changes in major parameters like diameter of particles, distance between particles and distance between two adjacent columns if changed how the system outcome changes.

2.2.1 Change of particle diameter

It is obvious that if the particle diameter is changed, change of radius of curvature, liquid thickness, permeability, porosity and saturation lead to the change in critical heat flux accompanying the temperature difference between the evaporator and condenser.

$$k = \frac{<\delta_w>}{d_p} \frac{\varepsilon^3 {d_p}^2}{180(1-\varepsilon)^2}$$

$$\varepsilon = 1 - \frac{2\pi}{\sqrt{3}{l_p}^2 <\delta_w>} [\frac{2}{3}(\frac{d_p}{2})^3 + (\frac{d_p}{2})^2 (<\delta_w> - \frac{d_p}{2}) - \frac{1}{3}(<\delta_w> - \frac{d_p}{2})^3]$$

$$<\delta_w> = \frac{1}{2}\{d_p(1+\cos\theta) - r_c[1-\cos(\theta-\theta_c)]\}$$

$$r_c = \frac{\frac{2}{\sqrt{3}} l_p - d_p \sin\theta}{2\sin(\theta-\theta_c)}$$

Here,

d_p = 56 μ m, l_p = 1.12 * d_p μ m, θ=101°C and θ_c =45°C

Above are the governing equations that are affected by the change of diameter (d_p) of the particle in the porous media. With the change of d_p, distance between particles (l_p) changes. With d_p and l_p changed, the fluid layer thickness (<δ_w>) over the porous media changes. Due to the change in d_p, l_p and <δ_w>, porosity (ε) changes and finally with all these changes, permeability, K changes. For the current study and current setup, diameter of the particles in the porous media has been changed. With this change and corresponding changes, heat flux versus temperature difference (between heater and condenser) graphs have been plotted. From these results it is clear that if the diameter of the particle is higher than 40 μ m, then that system can handle any temperature difference (from Δ T=1°C to Δ T=14°C) although the heat flux distribution is different for 40 μ m < d_p <43 μ m and same for d_p > 43 μ m but if the diameter of the particle is less than 40 μ m, then that system cannot withstand up to ΔT=14°C.

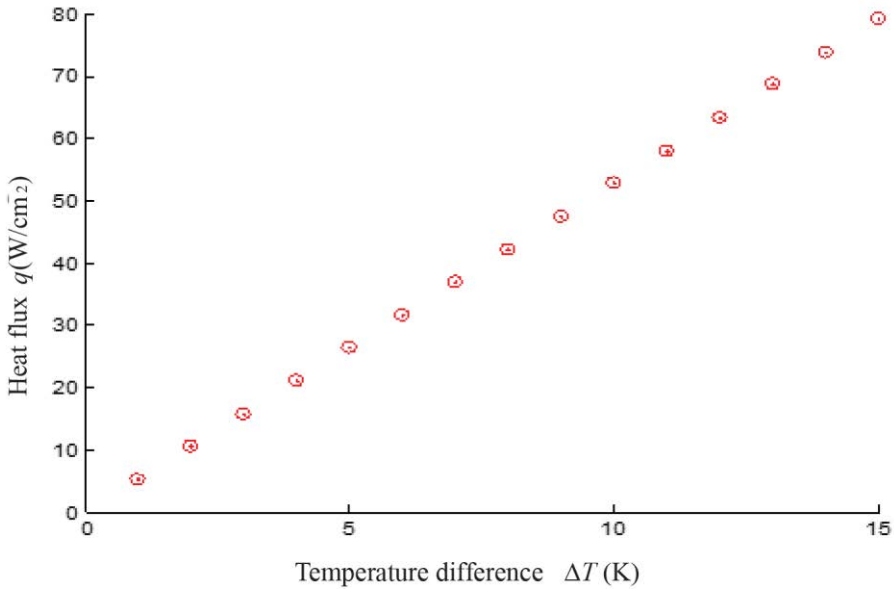

Figure 7 q (W/cm^2) versus ΔT for d_p = 43 μm or up

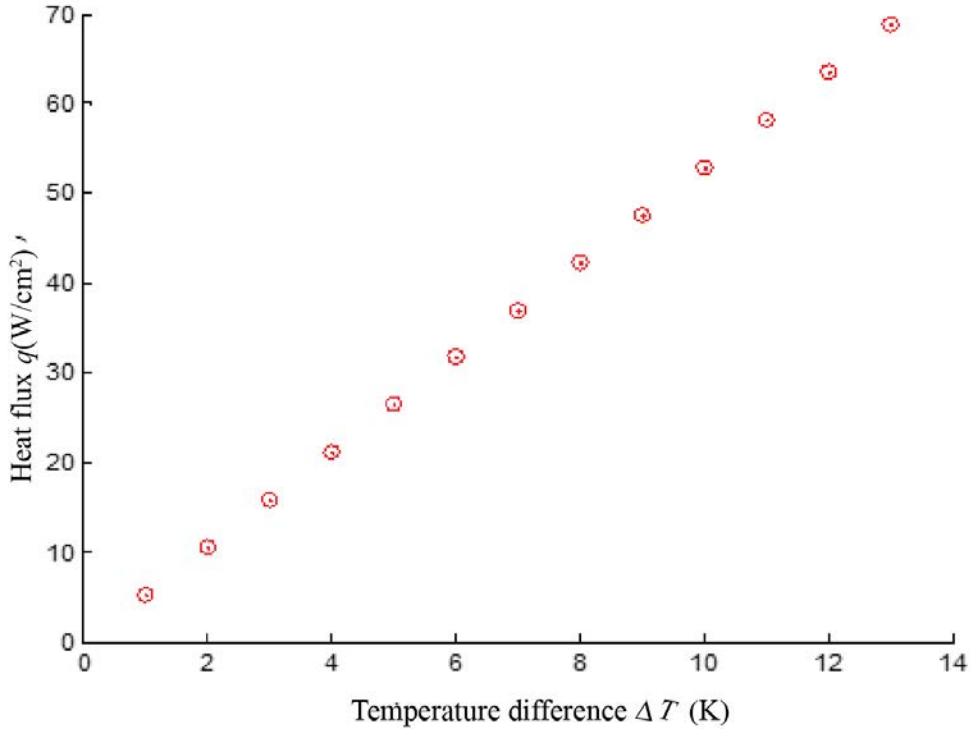

Figure 8 q (W/cm^2) versus ΔT for d_p = 42 μm, 41 μm and 40 μm

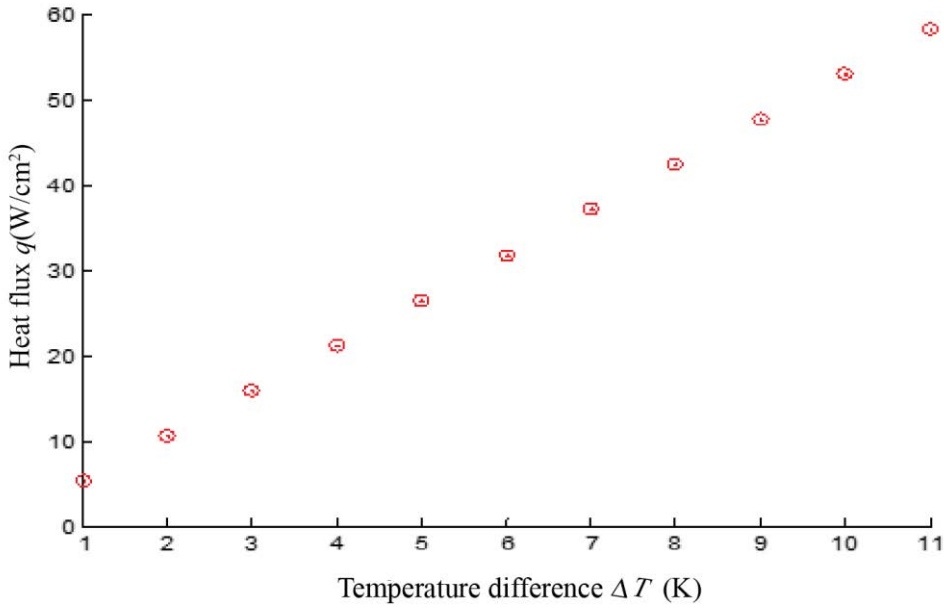

Figure 9 q (W/cm^2) versus ΔT for d_p =39 μm

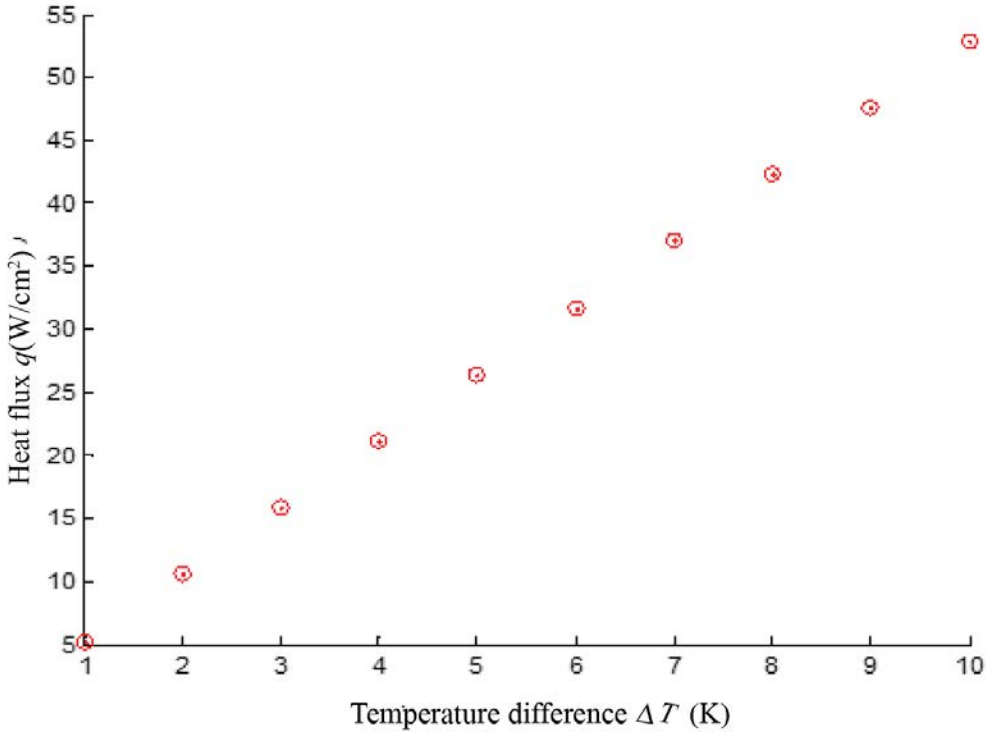

Figure 10 q (W/cm^2) versus ΔT for d_p =39 μm

So, from the graphs presented above it is clear that with the decrease of the diameter of the particle used in the porous media, the amount of heat transferred from the heater to the condenser as well as the range of temperature decreases.

2.2.2 Change of distance between particles

To know the outcome when the distance between particles changes, a thermal equilibrium model is considered which was analyzed using the program developed with Matlab.

$$k = \frac{<\delta_w>}{d_p}\frac{\varepsilon^3 {d_p}^2}{180(1-\varepsilon)^2}$$

$$\varepsilon = 1 - \frac{2\pi}{\sqrt{3}{l_p}^2 <\delta_w>}[\frac{2}{3}(\frac{d_p}{2})^3 + (\frac{d_p}{2})^2(<\delta_w> - \frac{d_p}{2}) - \frac{1}{3}(<\delta_w> - \frac{d_p}{2})^3]$$

$$<\delta_w> = \frac{1}{2}\{d_p(1+\cos\theta) - r_c[1-\cos(\theta-\theta_c)]\}$$

$$r_c = \frac{\frac{2}{\sqrt{3}} l_p - d_p \sin\theta}{2\sin(\theta - \theta_c)}$$

$$l_p = f \times d_p$$

Mathematical model of this calculation is the same as that presented for the change of diameter of the particles used in porous media. With the change of l_p (by changing f), r_c changes. With r_c, δ_w and with all these porosity and permeability changes. So, for this calculation, diameter is used from 43 μm to larger size, and it is observed for which l_p the heat pipe can handle higher heat flux as well as higher temperature difference.

For d_p=43 μm to 48 μm : if $\frac{l_p}{d_p}$ = 1.2 or more, the current setup can withstand up to 80W/cm^2 and can handle up to 14^{o}C temperature difference but if $\frac{l_p}{d_p}$ <1.2, this setup cannot withstand more than 70 W/cm^2 heat flux and not more than 13^{o}C temperature difference.

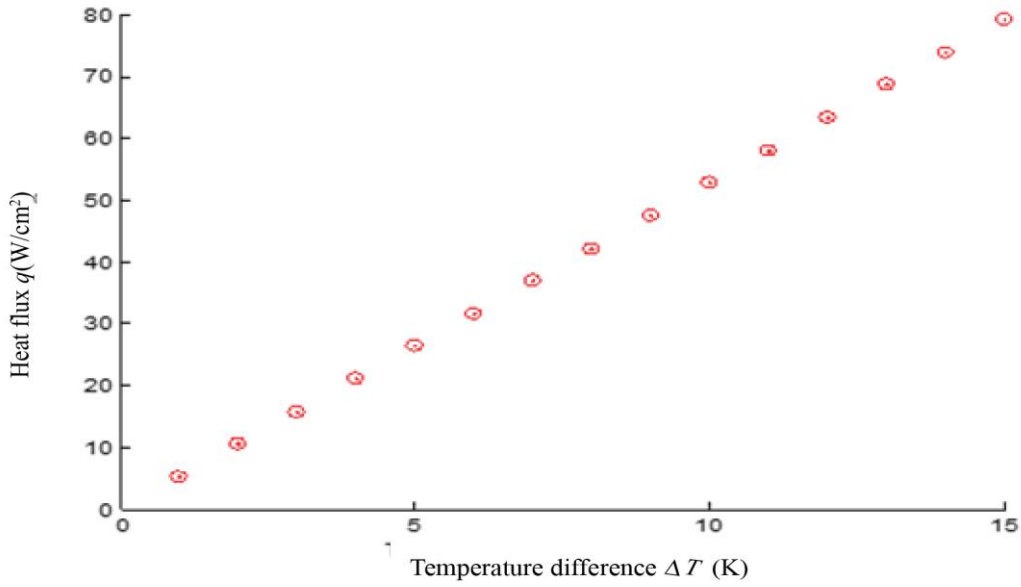

Figure 11 q(W/cm^2) versus ΔT (K) for d_p=43μm to 48μm l_p=1.2 d_p

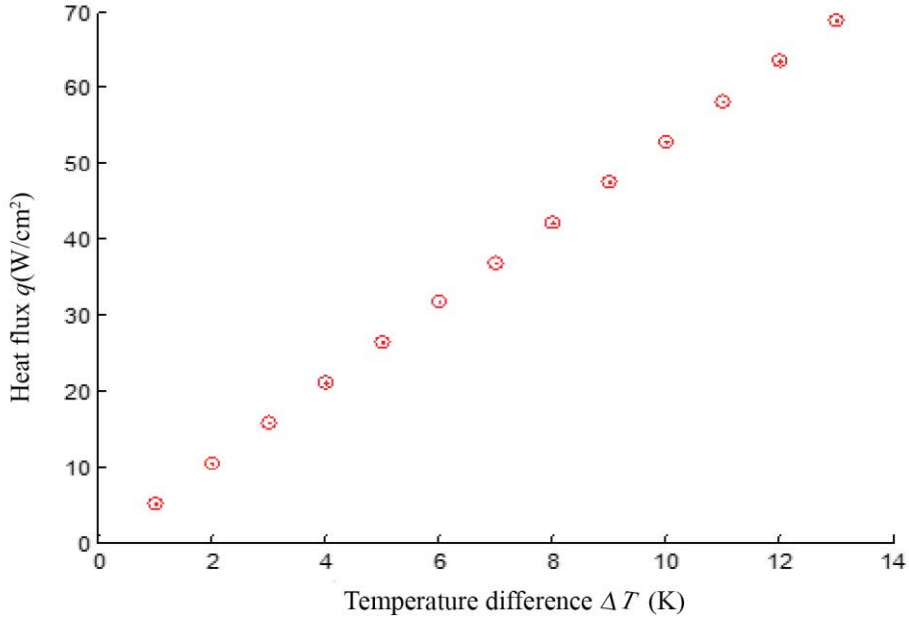

Figure 12 q(W/cm^2) versus ΔT for d_p=43 μm to 48 μm l_p =1.1d_p

For d_p=49 μm and above: if $\frac{l_p}{d_p}$ >= 1.1, the current setup can withstand up to 80W/cm^2 and can handle up to 14^{o}C temperature difference but if $\frac{l_p}{d_p}$ <1.11, this setup cannot withstand more than 70 W/cm^2 heat flux and not more than 13^{o}C temperature difference.

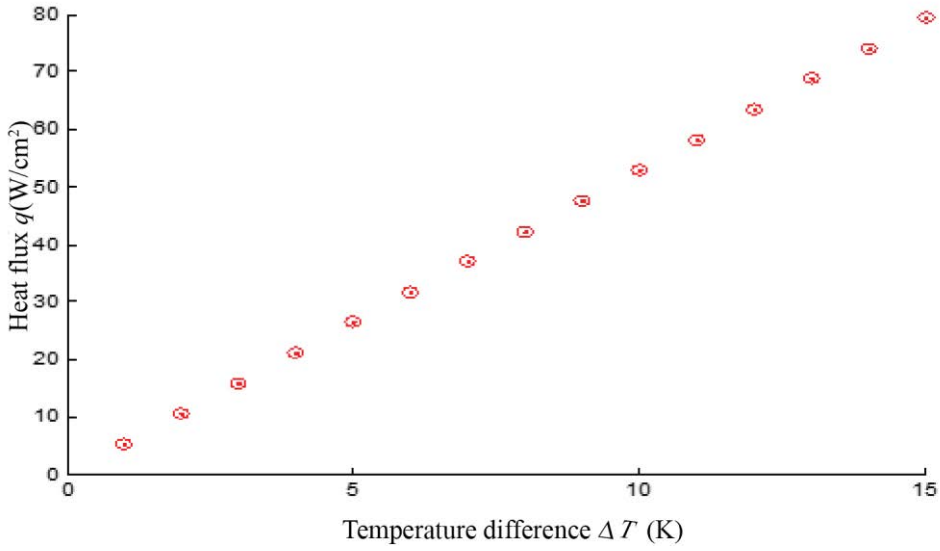

Figure 13 q (W/cm^2) versus ΔT for d_p=49μm and above l_p >=1.1d_p

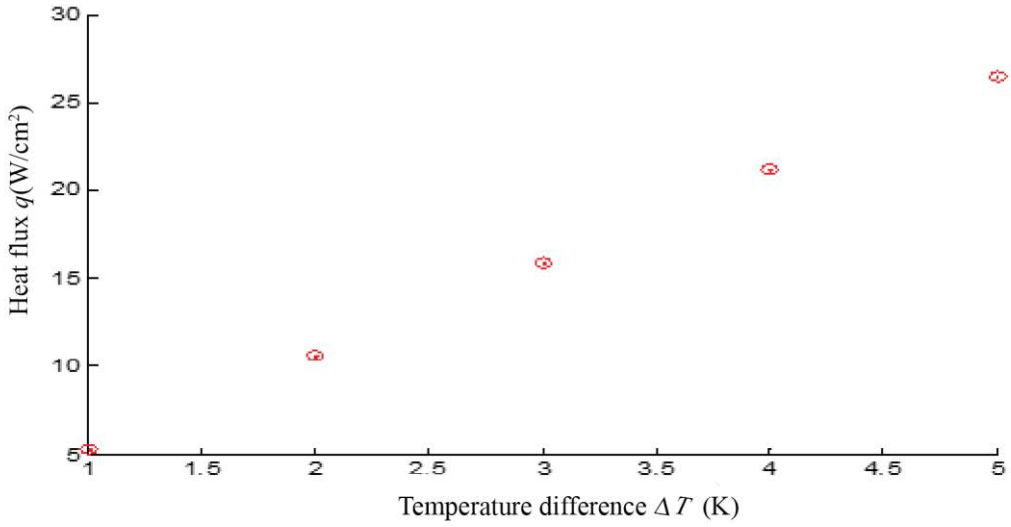

Figure 14 q(W/cm^2) versus ΔT for d_p=49μm and above l_p =1.0d_p

2.2.3 Change of distance between liquid arteries

Change of distance between two adjacent liquid arteries cause the reduction of length of flow in evaporator and condenser. It is considered that the distance between liquid arteries are always same. So changing distance means increasing the number of liquid arteries in the system. In addition, an addition of a new liquid column gives the heat pipe the capability of handling double amount of heat for the same temperature region. By changing diameter of particles and distance between particles, it is found that the optimal range of diameter is from 49 μm to above and the optimal distance between two adjacent particles is $1.1 \times d_p$ or more.

For d_p=49 μm, when two liquid arteries are considered, for $\frac{l_p}{d_p}$=1.1

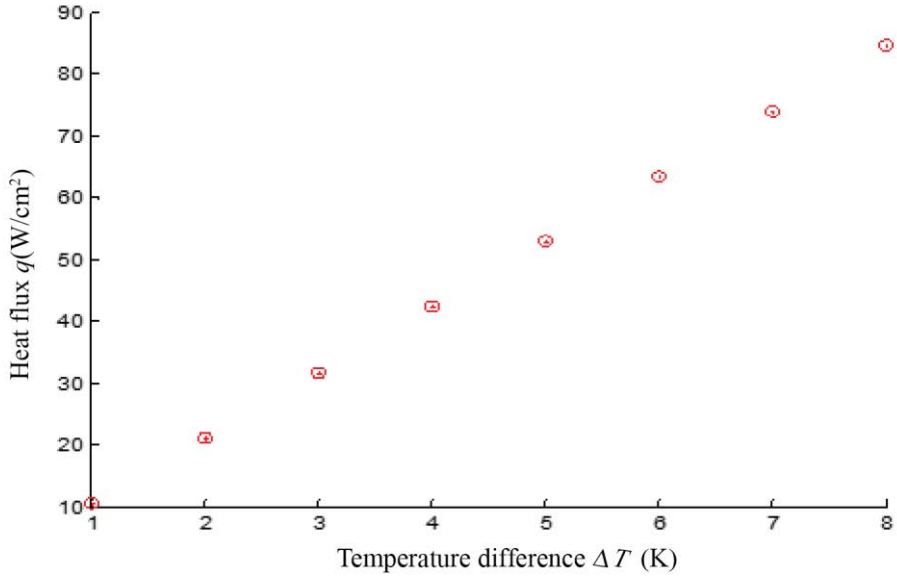

Figure 15 for d_p=49 μm and above l_p =1.1d_p for double artery

For d_p=49 μm , when two liquid arteries are considered, for $\frac{l_p}{d_p}$=1.2 and above,

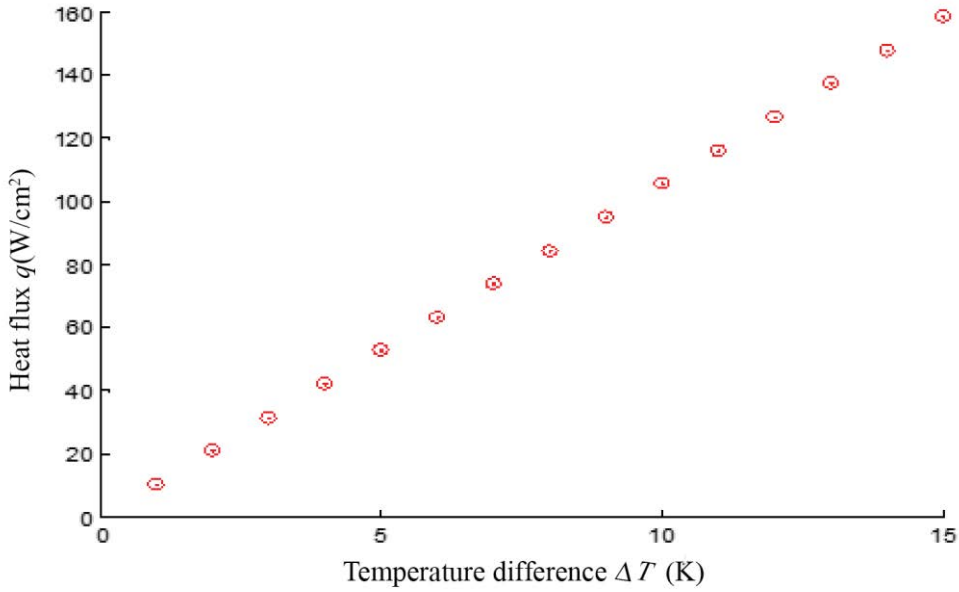

Figure 16 for d_p=49 μm and above l_p =1.2d_p for double artery

Now when 10 liquid arteries are used, heat flux increases incredibly but if $\frac{l_p}{d_p}$ is still 1.2 this

setup will not be able to handle up to 15ºC temperature difference.

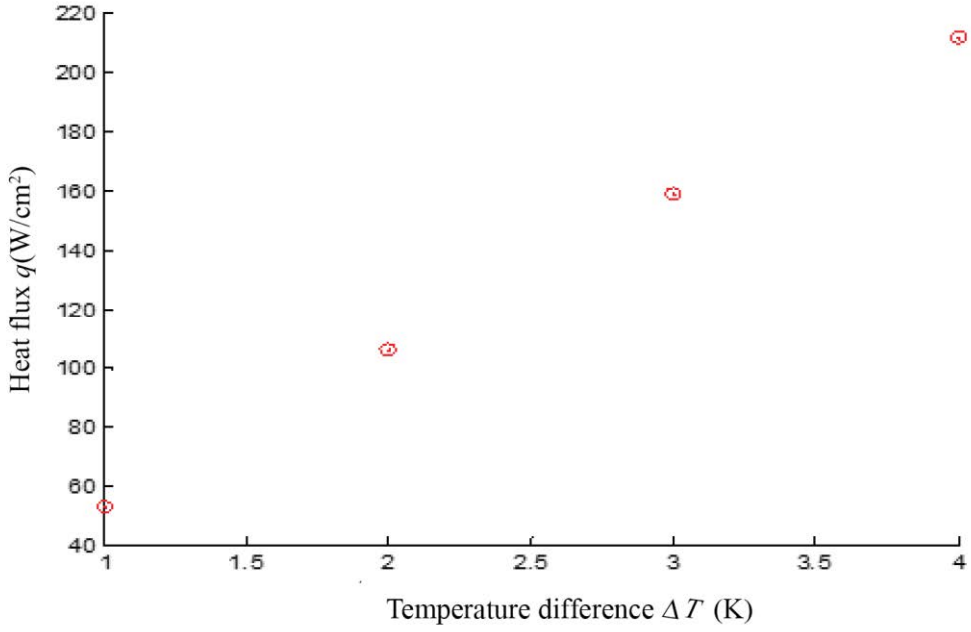

Figure 17 for d_p=49 μm and above l_p =1.2d_p for 10 arteries

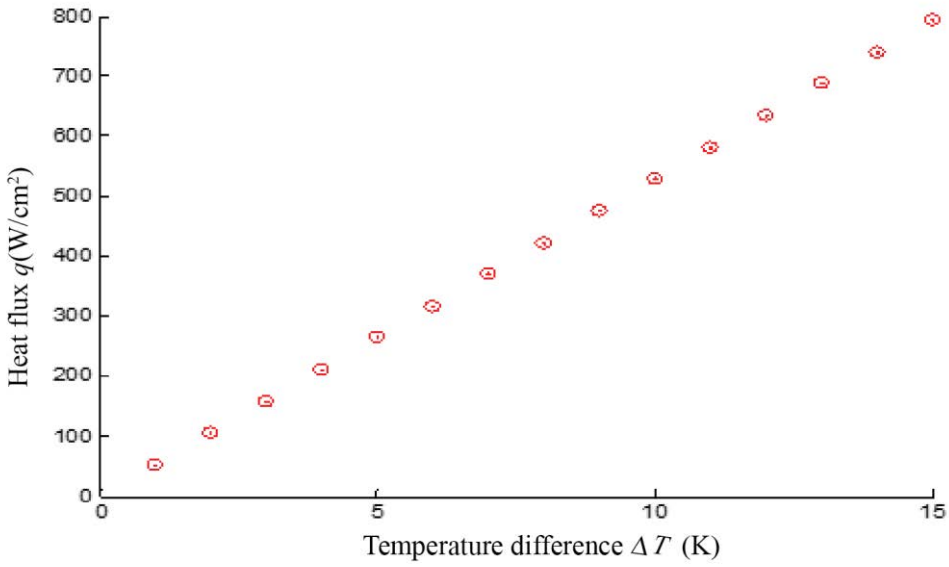

Figure 18 for d_p=49 μm and above l_p =1.5 d_p for 10 arteries

So, for handling a huge amount of heat increasing number of liquid arteries can yield better results although the distance between particles should be changed.

2.3 Results for Model Validation

In compatibility model, results are found using the equations that are already existing for the design parameters. In this case at least two variables are changed to see how the heat flux versus the temperature difference graph looks like. This study uses the existing equations. In the next section, parameters will be defined and derived to obtain more accurate and realistic results. To inspect the critical heat flux with the change in the diameter of the particles and distance between particles, used in the porous media of a heat pipe. For single and multiple artery heat pipes the temperature distribution along the heat flow path and the pressure distribution along the fluid flow path have been calculated previously. At this stage, it is important to learn about the change in critical heat flux with the maximum temperature difference between evaporator and condenser when the design parameters like diameter of particles and distance between two adjacent particles are changed.

$$k = \frac{< \delta_w >}{d_p} \frac{\varepsilon^3 {d_p}^2}{180(1-\varepsilon)^2}$$

$$\varepsilon = 1 - \frac{2\pi}{\sqrt{3}{l_p}^2 < \delta_w >} [\frac{2}{3}(\frac{d_p}{2})^3 + (\frac{d_p}{2})^2 (< \delta_w > - \frac{d_p}{2}) - \frac{1}{3}(< \delta_w > - \frac{d_p}{2})^3]$$

$$< \delta_w >= \frac{1}{2}\{d_p(1+\cos\theta) - r_c[1-\cos(\theta-\theta_c)]\}$$

$$r_c = \frac{\frac{2}{\sqrt{3}} l_p - d_p \sin\theta}{2\sin(\theta-\theta_c)}$$

$$l_p = f \times d_p$$

Limiting Criteria for dry-out: $\Delta P < \frac{2\sigma}{r_c}$

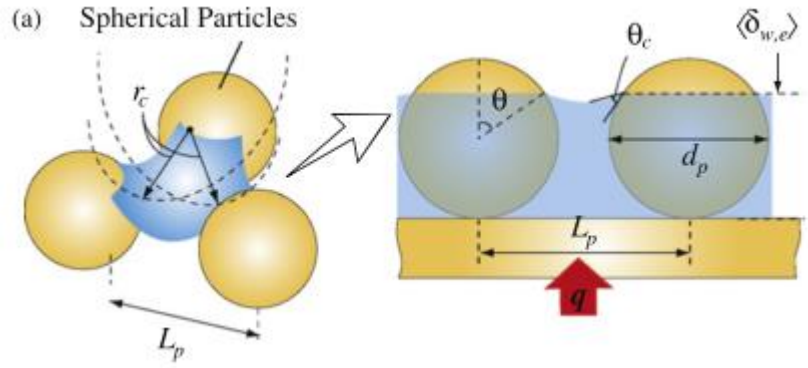

Figure 19 A schamatic of the monolayer wick including key geometrical parameters [3]

Table 2 Result for model validation

Diameter	l_p/d_p	q_{CHF} (W/cm^2)	Temperature Difference ΔT(K)
30μm	1	36.61	1
	2	934.38	20
	3	7748.20	120
60μm	1	95.20	4
	2	1854.80	56
	3	15573.00	286
90μm	1	410.48	17
	2	2796.62	109
	3	23399.00	497

By changing the diameter of particles and the distance between the particles, considering the dry-out criteria, the following results are found from the Matlab simulation. It is likely that with the increase of diameter Critical Heat Flux increases and the heat pipe can handle greater range of temperature. The same trend is followed when the distance between the particles is increased.

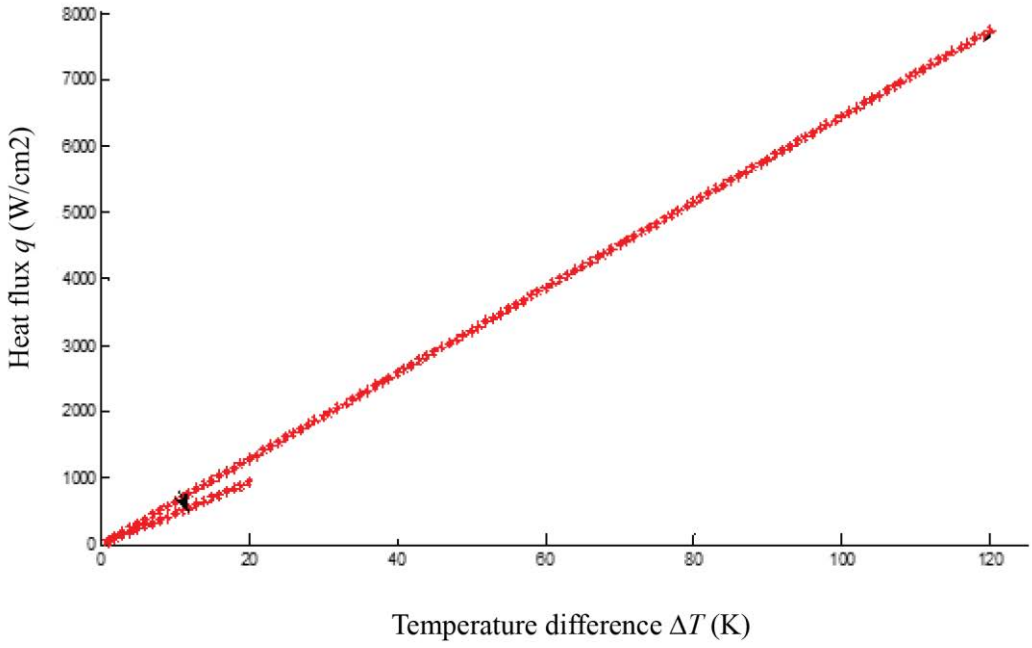

Figure 20 Heat flux versus temperature difference for d_p=30μm and l_p/d_p=1,2,3(l_p/d_p =1 is not visible in this figure but presented in the following figure.)

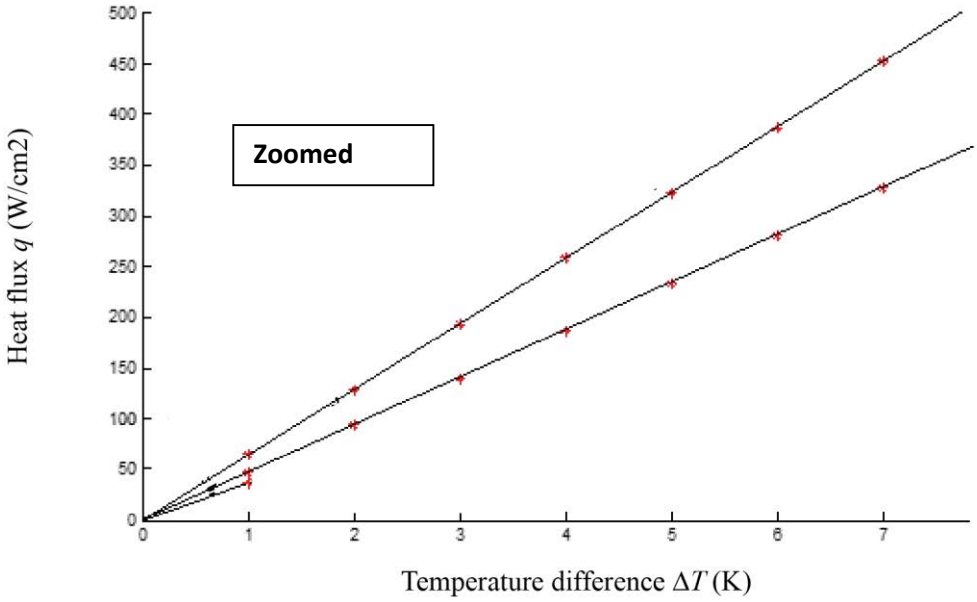

Figure 21 Heat flux versus temperature difference for d_p=30μm and l_p/d_p =1,2,3 (Zoomed)

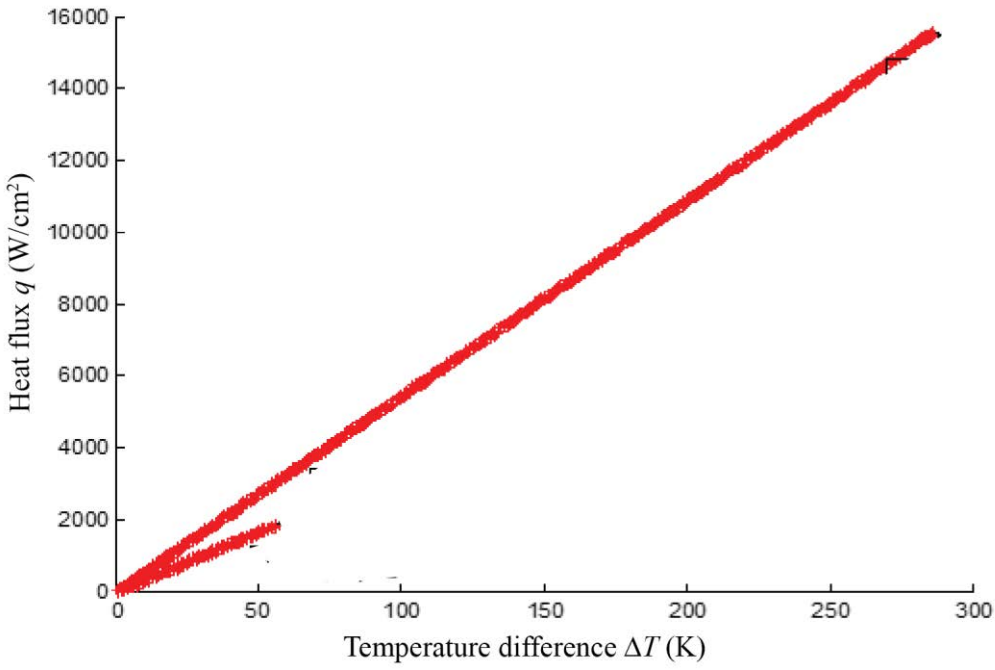

Figure 22 Heat flux versus temperature difference for d_p = 60μm and l_p/d_p =1,2,3(l_p/d_p =1 is not visible in this figure, presented in the following figure.)

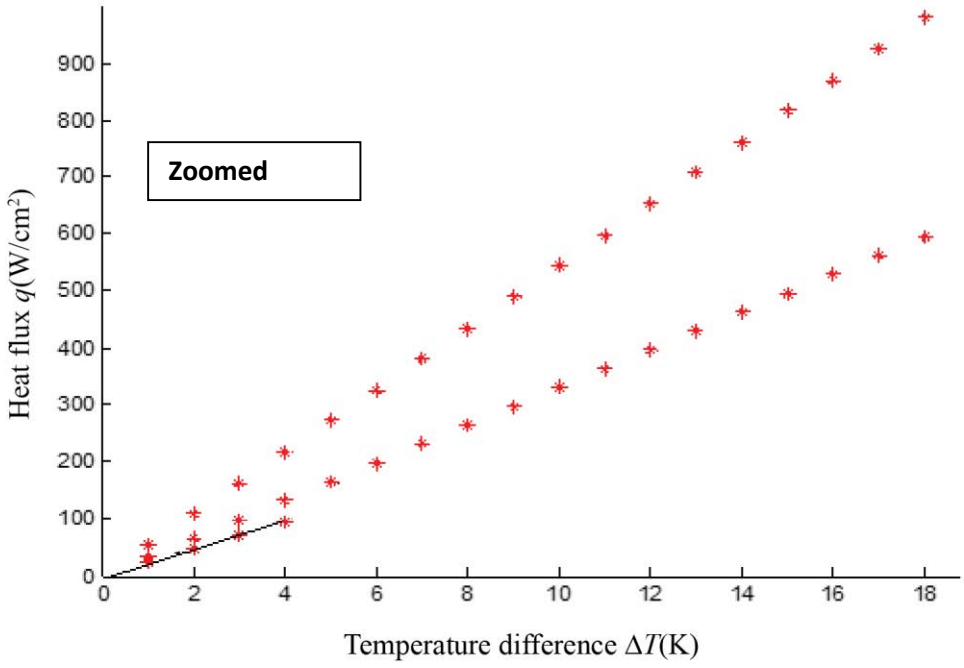

Figure 23 Heat flux versus temperature difference for d_p =60μm and l_p/d_p =1,2,3(l_p/d_p =1 is the black line.)

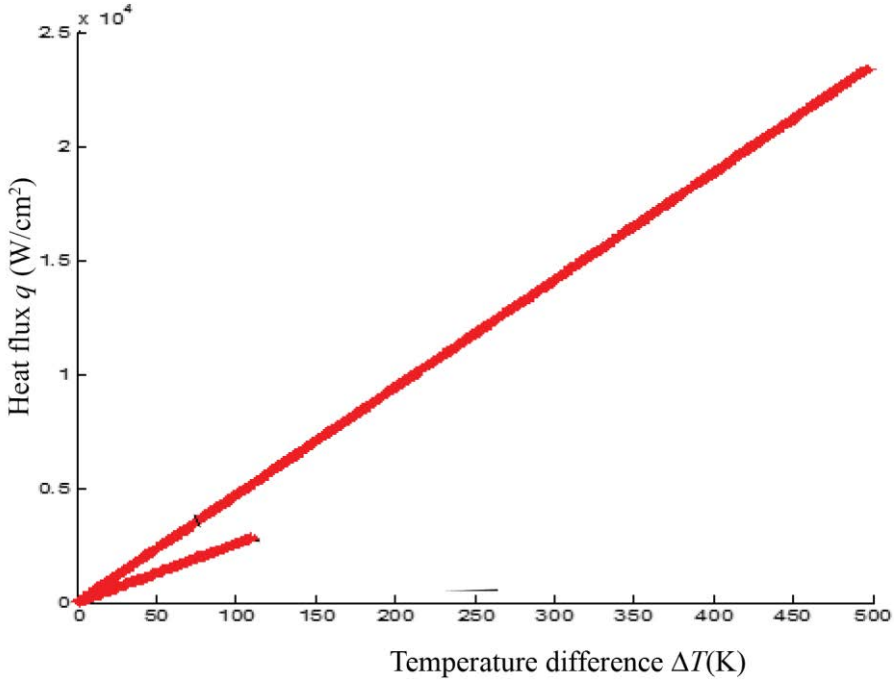

Figure 24 Heat flux versus temperature difference for d_p =90μm and l_p/d_p =1,2,3 (l_p/d_p =1 is not visible here but it will be presented in the following figure)

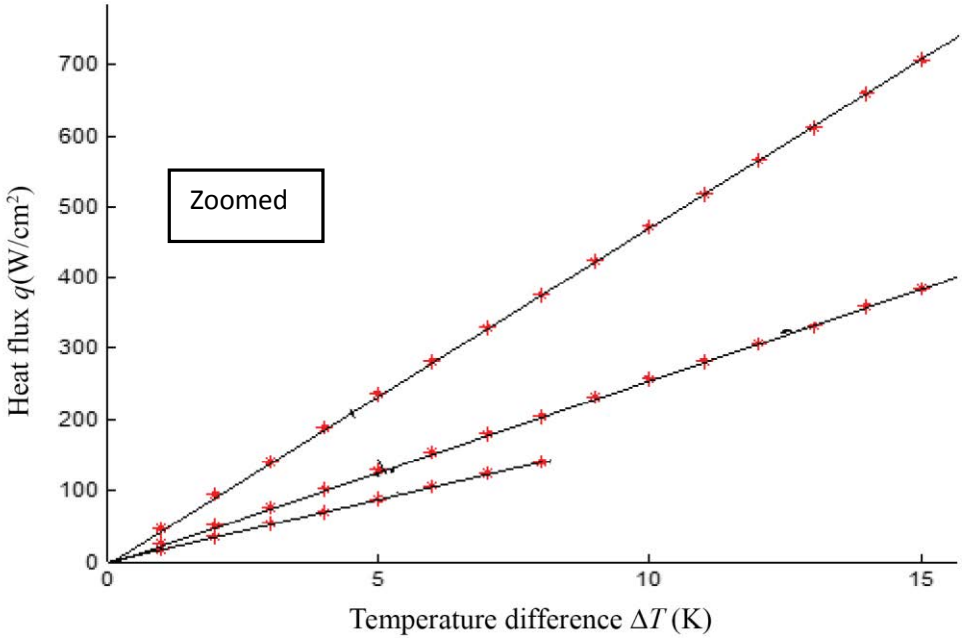

Figure 25 Heat flux versus temperature difference for d_p=90μm and l_p/d_p=1,2,3 (Zoomed)

2.4 Thermal Equilibrium Model Simulation

2.4.1 Structure

Physical model structure consists of three major parts, i.e., evaporator with thin monolayer wick, porous post or column and condenser with porous bed. Particle diameter of 60 μm is used in both evaporator and condenser wicks. Bigger particles are used in the posts. Monolayer porous structure is included in this prototype where working fluid is fed into the spaces between particles. 1cm×1cm heater is the main heat source of this model. Evaporator monolayer is considered first only for simplicity to find the heat flux. As long as the critical heat flux is obtained from the monolayer only, liquid arteries and condenser are added gradually to find out the overall critical heat flux of the system in total.

2.4.2 Heat Transfer

Heat supplied by the heater at the bottom transfers through the copper body, and monolayer wick, and then is consumed by the evaporation by the working fluid. The role of the wick is to provide the working fluid to the heated surface and to minimize the thermal resistance. The main goal of this study is to optimize the monolayer wick structure to enhance the heat transfer rate and minimize the thermal resistance.

2.4.3 Fluid Flow

Evaporated working fluid (water) gets condensed in the condenser. Condensed water comes back to the evaporator through liquid column or artery. Artery is made with bigger particles which hinder fluid flow. So there is flow resistance in the liquid artery. Fluid flow is important in this model because if ample amount of working fluid doesn't come back to the evaporator wick before the evaporator dries out, heat transfer will stop immediately. So maintaining the pressure difference below the critical value is also important otherwise the whole system will become a fiasco and no water would available for further evaporation. Permeability is a key parameter for fluid flow. In this study three models for permeabilities are used for design optimization.

2.4.4 Physical Model

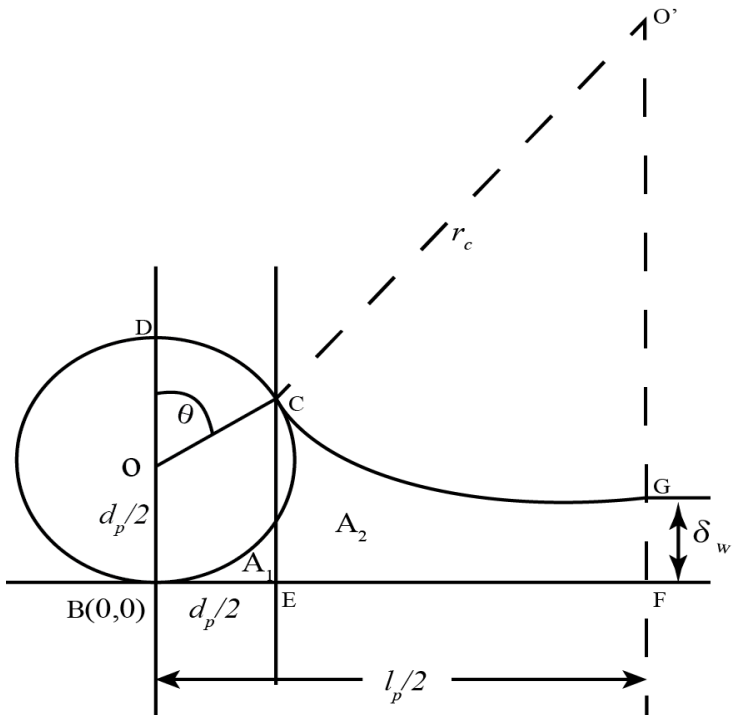

Figure 26 Physical model of the single particle with liquid geometry

Figure 26 represents the physical model geometry. This is considered as the unit cell for the monolayer wick. Here O centered BCD is the micro particle. At point C working fluid touches the particle. BF is haft the distance of two adjacent particles. GF stands for the liquid thickness and CG is the curvature of the working fluid. O'C and O'G are the radius of the curvature and DOC represents the angle to the liquid contact. Throughout the whole study, contact angle is assumed constant 45^o. OB, OC or OD represent radius of the particle. It is assumed that all the boundaries except the bottom one and the liquid surface are insulated in this physical model. With the increase of heat, temperature of the bottom boundary BF increases and working fluid gets evaporated from the surface and the liquid thickness GF decreases gradually. As a result value of the angle to the liquid contact DOC increases to its maximum. When the system reaches to the critical heat flux, maximum heat flux is obtained and then working fluid gets evaporated very quickly leading to the system towards chocking. If the pressure difference between the evaporator and condenser is higher than the critical value, chocking may occur

before reaching the maximum heat flux. Based on the physical model demonstrated in figure 26, all the parameters are calculated.

2.4.5 Mathematical Model

For mathematical model, following equations are used.

I. Heat transfer rate is calculated by the Fick's law, i.e.,

$$q = -k\nabla T$$

Where, q is the heat flux density, k is the thermal conductivity and T is the temperature. Fick's law is a key to determine the heat flux due to conduction. Here effective thermal conductivity is calculated by the relation [3] given as

$$k_e = k_w(k_s / k_w)^{0.28-0.757\log_{10}\varepsilon-0.057\log_{10}(k_s/k_w)}$$

II. Viscous pressure drop of the liquid working fluid is calculated by the Darcy's law,

$$\Delta p = -\frac{\mu}{K} < u_l > L$$

Where Δp is pressure gradient, K is the permeability, μ is the liquid viscosity, L is the characteristic length. No liquid pressure drop by the inertia is considered since the liquid velocity is negligibly small.

III. Capillary pumping capability is calculated by Young-Laplace equation,

$$p_v - p_l = 2\sigma(\frac{1}{r_{c,e}} - \frac{1}{r_{c,c}})$$

Where p_v - p_l is the pressure difference between vapor and liquid sides, σ is the surface tension $r_{c,e}$ is the capillary meniscus at evaporator surface and $r_{c,c}$ is the capillary meniscus at condenser

surface. Here, $r_{c,c}$ is considered to be infinity since the condenser is typically fully flooded during the operation, and this reduces the above equation to

$$(p_v - p_l)_{\max} = \frac{2\sigma}{r_c}$$

IV. Governing equation: The liquid velocity is given as $< u_l >= \frac{\dot{m}}{\rho A}$ where $\dot{m}$ is mass flow rate. From Darcy's law and Young-Laplace equation, we find:

$$\frac{2\sigma}{r_c} = \frac{\mu}{K}\frac{L\dot{m}}{\rho A}$$

So, $\dot{m} = \frac{2\sigma}{r_c} \times (\frac{K\rho A}{\mu L})$

The heat transfer rate, Q is related to the mass flow rate and latent heat, $Q = \dot{M} \times \Delta h_{\lg}$ and $\dot{M} = \dot{m} \times A_h$.

So, $q = \dot{m} \times \Delta h_{\lg}$. Thus,

$$q_{CHF} = \frac{2\sigma}{r_c} \times \frac{\rho}{\mu} \times (\frac{L}{KA})^{-1} \times \Delta h_{\lg}$$

V. Monolayer model: For monolayer, the governing equation changes to

$$q_{CHF} = \frac{2\sigma}{r_c} \times \frac{\rho}{\mu} \times (\frac{l_m}{K_m A_m})^{-1} \times \Delta h_{\lg}$$

Here $A_m = 4\delta_w \times$ cross-section area of liquid and absolute permeability [3],

$$K_m = \frac{\varepsilon^3 d_p^{\,2}}{180(1-\varepsilon)^2}$$

In absolute permeability K, saturation S (volume occupied by water divided by the pore volume) is not considered. In this study, saturation is included with permeability and three different models are used to find out which relationship gives the best result.

I. $K_r=K$, relative permeability K_r is equal to the absolute permeability K

II. $K_r=SK$, linear relationship between relative permeability K_r and absolute permeability K

III. $K_r=S^3K$, nonlinear relationship between relative permeability K_r and absolute permeability K

Therefore, it is obvious that, for the design optimization, parameters i.e. radius of curvature (r_c), liquid thickness (δ_w), porosity (ε) and relative permeability (K_r) need to be derived geometrically.

2.4.5.1 Radius of curvature (r_c)

In Figure 27, B centric GCM is considered as a particle and hashed part depicts working fluid. Figure 27 represents half of a pore (symmetry). C is the contact point of water and particle so ZZ' is the tangent. $\angle$ ZBC = $\angle$ ABC = $\angle$ CQN = θ, angle to the contact point. O is the center of liquid curvature so, OC = ON = r_c. EF is the tangent to the water surface. $\angle$ ECZ = $\angle$ FCZ' = θ_c. To find the radius of curvature $r_{c,\angle\beta}$ is needed. Here radius of curvature is the O centered CN curvature, which shows the upper surface of working fluid inside the pore.

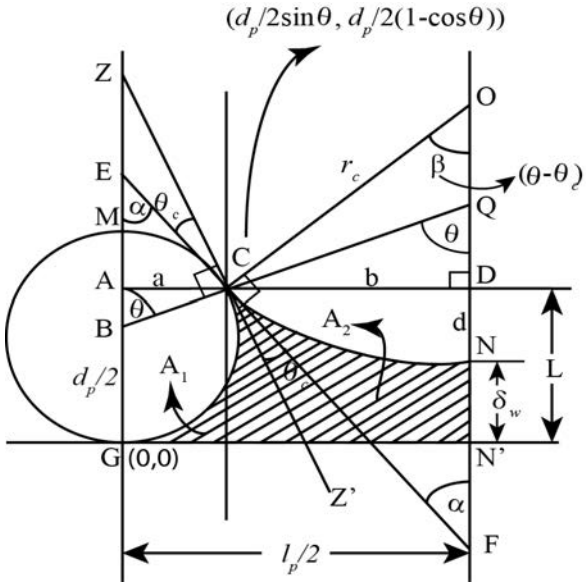

Figure 27 Particle and half pore geometry including the various lengths and angles for the mathematical models to find $\angle\beta$, we start from ΔEBC,

$90^o - \theta_c + \theta + \alpha = 180^o \Rightarrow \alpha = 90^o - (\theta - \theta_c)$,

ΔOCF, $\beta + \alpha + 90^o = 180^o \Rightarrow \beta = 90^o - \alpha \Rightarrow \beta = \theta - \theta_c$.

From ΔABC, $\angle ACB = (90^o - \theta)$. So, $a = \frac{d_p}{2}\sin\theta$.

From, ΔOCD,

b= $r_c \sin(\theta - \theta_c)$

$\Rightarrow r_c = \frac{b}{\sin(\theta-\theta_c)} = \frac{FE-a}{\sin(\theta-\theta_c)} = \frac{l_p - d_p\sin\theta}{2\sin(\theta-\theta_c)}$ So, we obtain

$$r_c = \frac{l_p - d_p\sin\theta}{2\sin(\theta-\theta_c)}$$

2.4.5.2 Liquid thickness, δ_w

Liquid thickness is calculated as the distance of water from the evaporator wick bottom, which is NN' in Figure 27. Here, DN' = L = AG = AB + BG = AB + $\frac{d_p}{2} = \frac{d_p}{2} + \frac{d_p}{2}\cos\theta$.

Liquid thickness is given as

$$\delta_w = \text{L - d} = \text{L - (}\ r_c - OD\ \text{)} = \text{L - (}\ r_c - r_c\cos(\theta - \theta_c)\ \text{)} = \frac{d_p}{2}(1+\cos\theta) - r_c(1-\cos(\theta-\theta_c))$$

2.4.5.3 Porosity

Porosity of one of the critical parameters to control the effective thermal conductivity, permeability, which are directly related to the fluid and thermal transport. Porosity $\varepsilon(\theta)$ is the ratio of pore volume to the box volume i.e. ratio of open space for working fluid compared to the total volume. Control volume is, $V = d_p l_p^2$, pore volume is $V_p = V - \frac{4}{3}\pi(\frac{d_p}{2})^3$, and porosity is

$$\varepsilon(\theta) = \frac{V_p}{V} = 1 - \frac{1}{6}\pi(\frac{d_p}{l_p})^2$$

2.4.5.4 Saturation *S*

The saturation, *S*, is the volume occupied by water and pore volume as given as

$$S = \frac{V_w}{V_p}$$

Finding volume occupied by water V_w is performed for, $\theta > 90$, from Figure 27,

A_1:

$\int_0^{\frac{d_p}{2}\sin\theta} (\frac{d_p}{2}dx - \sqrt{(\frac{d_p}{2})^2 - x^2})dx$; Let, $x = \frac{d_p}{2}\sin\lambda$

$A_1 = \int_0^{\frac{dp}{2}\sin\theta} \frac{d_p}{2}dx - \int_0^{\theta} \sqrt{(\frac{d_p}{2})^2 - (\frac{d_p}{2}\sin\lambda)^2}\cos\lambda d\lambda$

$= \int_0^{\frac{d_p}{2}\sin\theta} \frac{d_p}{2}dx - \int_0^{\theta} \frac{d_p}{4}(1+\cos 2\lambda)d\lambda$

$= (\frac{d_p}{2})^2 \sin\theta - \frac{d_p}{4}\theta - \frac{d_p}{4}\frac{\sin 2\theta}{2}$

A_2:

$\int_{\frac{d_p}{2}\sin\theta}^{\frac{l_p}{2}} (r_c + \delta_w - \sqrt{(r_c^2 - (x - \frac{l_p}{2})^2)})dx$;

Let, $x - \frac{l_p}{2} = r_c \sin\lambda$ and $\zeta = \sin^{-1}(\frac{r_c}{2}(\mathrm{d}_p \sin\theta - \mathrm{l}_p))$

$A_2 = \int_{\frac{d_p}{2}\sin\theta}^{\frac{l_p}{2}} (r_c + \delta_w)dx - \int_{\zeta}^{0} r_c^2 \cos^2\lambda d\lambda$

$= [(r_c + \delta_w)(\frac{l_p}{2} - \frac{d_p}{2}\sin\theta) - \frac{r_c^2}{2}] \times [\sin^{-1}\{\frac{r_c}{2}(d_p \sin\theta - l_p)\} - \sin[2(\sin^{-1}\{\frac{r_c}{2}(d_p \sin\theta - l_p)\})]]$

Total area, A = A1+A2, when $\theta < 90$, the part of area of the particle which is right to the normal through C needed to be subtracted from the total area.

Part of area right to the normal through C,

$$A_d = \frac{2(90-\theta)}{360} \times \pi(\frac{d_p}{2})^2 - \frac{d_p}{2}\sin\theta \times \frac{d_p}{2}\cos\theta$$

So in this case the area occupied by water for the half pore is: (A-A_d)

Therefore the area (occupied by water),

A_w=A (for $\theta > 90^0$) and A_w=A-A_d (for $\theta < 90^0$), Thus

$$V_w = A_w \times l_p .$$

2.4.6 Parametric Studies

Key properties are calculated here using the above-mentioned relations. Here solid liquid contact angle is considered constant θ_c=45° throughout the whole study.

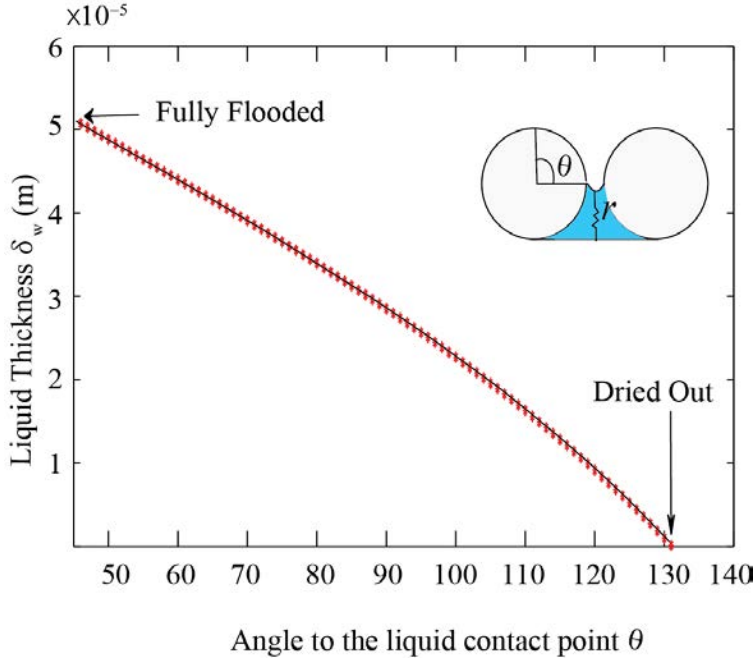

Figure 28 Liquid thickness δ_w (m) versus angle to the liquid contact θ

Figure 28 illustrates that liquid thickness (δ_w) decreases almost linearly until the dry-out occurs (θ = 131°) which is expected because with the decrease of water level, liquid thickness should decrease.

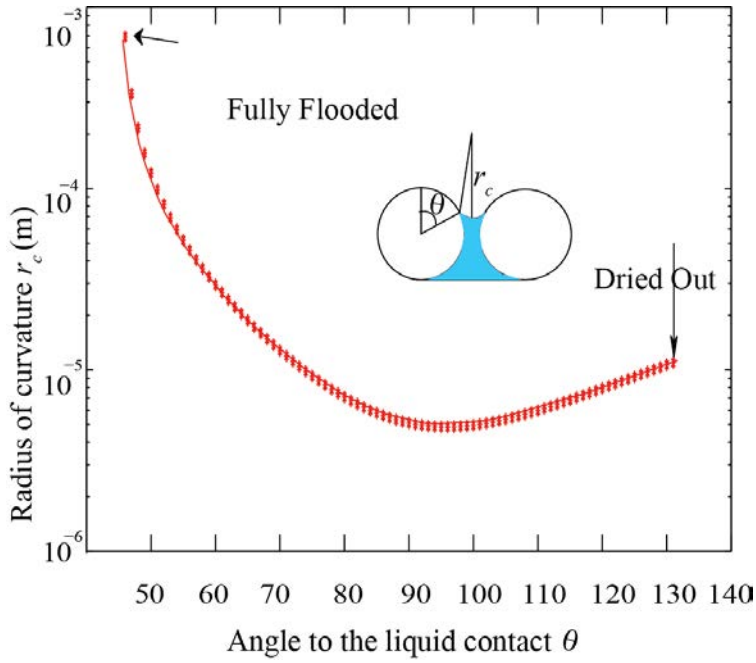

Figure 29 Radius of curvature r_c (m) versus angle to the liquid contact θ

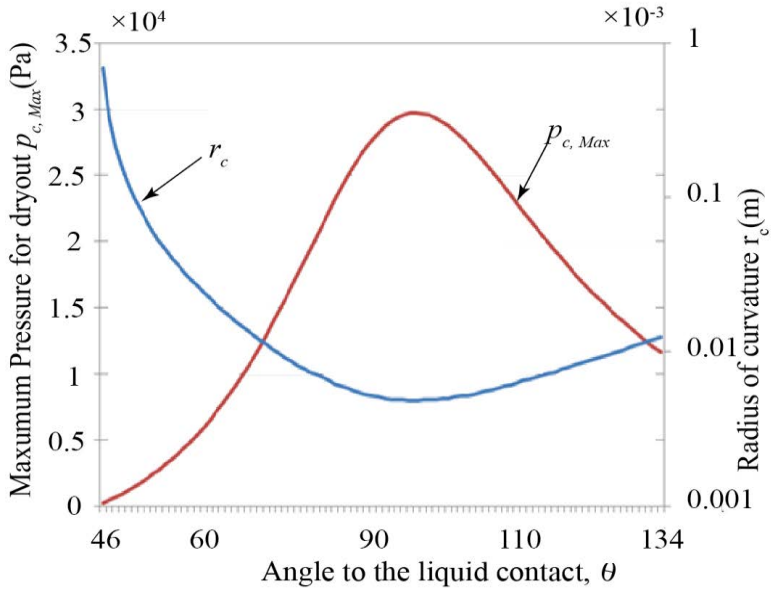

Figure 30 Maximum pressure for dry-out p_c,max (Pa) and radius of curvature r_c (m) versus angle to the liquid contact θ

Figure 29 shows that, radius of curvature (r_c) decreases from very high value to a minimum and then starts increasing slightly with θ. The minimum value of radius of curvature (r_c) for

which maximum heat flux is obtained is 5.09μm. In Figure 30 maximum pressure (p_c) and radius of curvature (r_c) is plotted against angle to the liquid contact (θ).

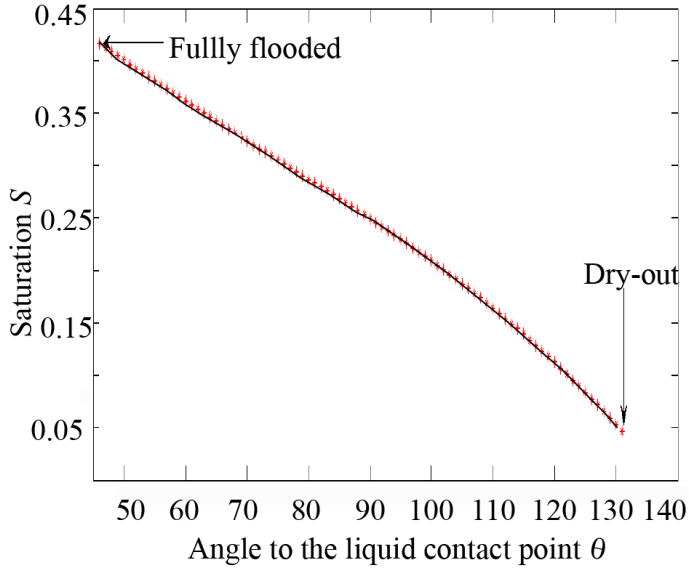

Figure 31 Saturation S versus angle to the contact point θ

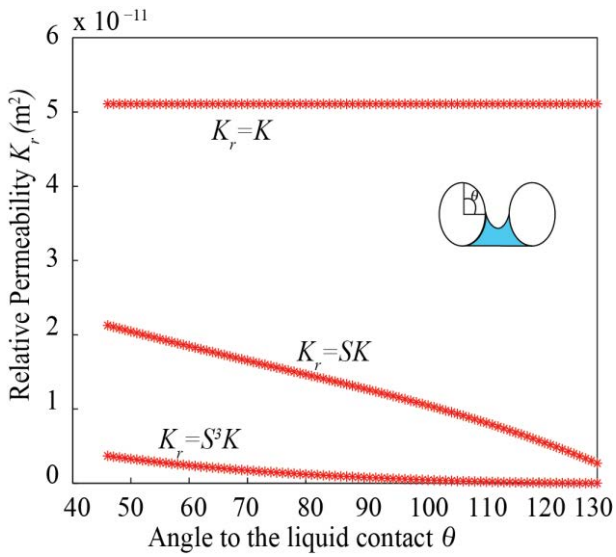

Figure 32 Three Relative permeability K_r (m^2) models with respect to the angle to the liquid contact θ

Saturation (S) versus angle (θ) is depicted in Figure 31 where maximum saturation is 0.43 which validates the saturation formula developed. Relative permeability (K_r) being a function

of saturation decreases with angle to water contact θ shown in Figure 32. Here particle diameter d_p = 60μm and distance between adjacent particles is l_p = 1.12 × d_p.

2.5 Results and Discussions for Thermal Equilibrium Simulation

2.5.1 Results for Monolayer Wick Only

First one with monolayer only, second one contains an artery along with the evaporator monolayer and finally the third model consists of evaporator monolayer, liquid artery and condenser monolayer. It is considered that the heat transfers from heater to the evaporator wick, then to the monolayer wick having diameter of 60 μm. Maximum heat flux $q_{CHF} = 1461.8$ W/cm^2 is obtained for the minimum value of radius of curvature r_c = 688.72 μm, while minimum heat flux only $q_{CHF} = 19.23$ W/cm^2 is obtained for the maximum value of radius of curvature $r_c = 5.09 \times 10^{-6}$ m. From the value of maximum critical heat flux it might seem that the value is comparatively big but while validating the second and third part of the model when resistance due to liquid artery and resistance due to the monolayer present in the condenser are considered, the maximum critical heat flux will come down. Effective thermal conductivity measured in this study is k_e = 5.253 W/m-K and the porosity is ε = 0.5826. Absolute permeability calculated is $K = 2.270 \times 10^{-11}$ m^2.

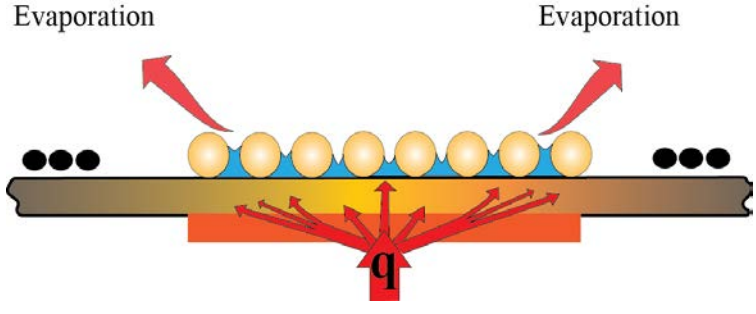

Figure 33 Model with evaporator monolayer only

To understand the limit of the systems and validations, the performance is calculated in the three consecutive steps (monolayer wick only, monolayer-liquid artery, and monolayer-liquid

artery-condenser). The effects of the geometries of the monolayer wick on the performance are shown below.

Table 3 Numerical results for monolayer only

Parameters	Description	Minimum heat flux	Maximum heat flux
r_c, m	Radius of curvature	688.72e-6	5.09e-6
δ_w, m	Liquid thickness	50.735e-6	28.5e-6
R K/(W/cm^2)	Resistance	0.0966	0.0543
q, W/cm^2	Heat flux	19.23	1,461.8
ΔT, °C	Temperature gradient	1.857	79.33
θ	Angle to the liquid contact	46	90

2.5.2 Result for monolayer and liquid artery

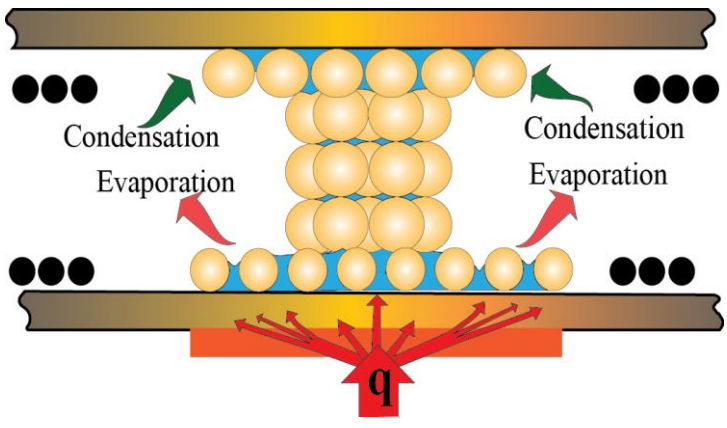

Figure 34 Model with evaporator monolayer and liquid artery and condenser wick

In this case condenser wick is also included in the calculation. d_p = 200μm particle is also used for condenser wick and $l_p = 1.12d_p$. Permeability $K_r = 2.252\times10^{-10}$ m^2, and porosity $\varepsilon = 0.582$. Obtained maximum heat flux q_{CHF} = 885.44 W/cm^2.

Liquid artery is added with the previous model. In order to ensure ample liquid supply through the artery, particle size is increased to 200 μm.

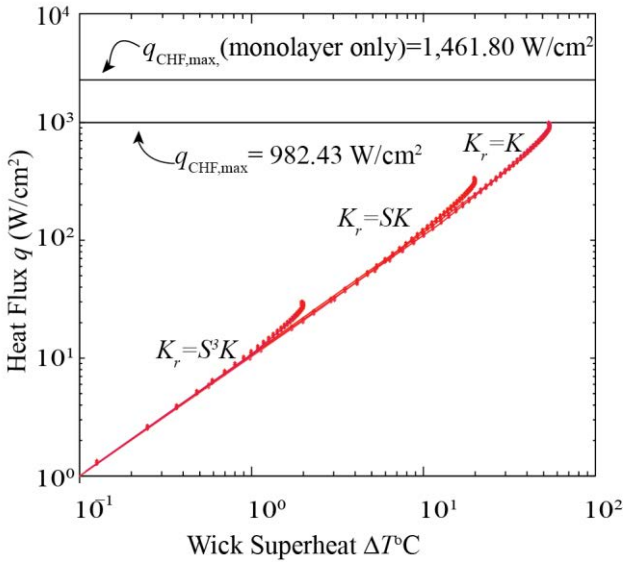

Figure 35 Heat flux q_{CHF} W/cm^2 as a function of the wick superheat ΔT (K)

For the feasibility of manufacturing the liquid penetration length is considered as 1cm. $q_{CHF,max}$ = 982.43 W/cm^2 for absolute permeability. Like monolayer only, when permeability is a function of saturation, maximum critical heat flux decreases.

2.5.3 Particle distance effect

The heat flux q(W/cm^2) is calculated with respect to the wick superheat for different l_p (distance between the adjacent particles), as shown in Figure 36. As the l_p increases, the maximum heat flux increases, while the thermal resistance decreases. As the distance increases the porosity increases and the liquid permeability increases, but the capillary pumping capability decreases, thus, the performance decreases. Also, the thermal resistance increases due to the significant water (low thermal resistance).

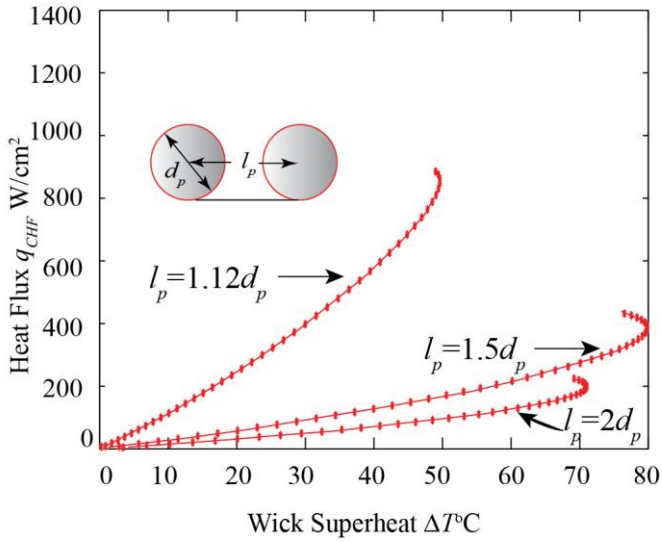

Figure 36 Heat flux q_{CHF} W/cm^2 versus the wick superheat ΔT (K)

2.5.4 Particle size effect

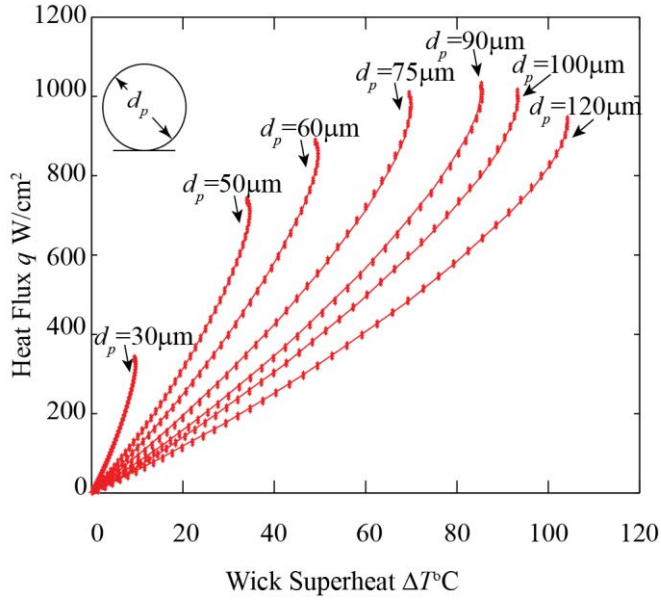

Figure 37 Heat flux q (W/cm^2) versus the wick superheat ΔT(K)

When heat flux q (W/cm^2) is calculated as a function of the particle size (d_p) used in the monolayer, with the change in particle size, different range of heat flux and temperature differences are found. It is seen from Figure 37 that if the particle size increases, heat flux keep increasing until it reaches to $d_p = 90$ μm. After $d_p = 90$ μm, heat flux starts decreasing. But with the increase in particle size, the wick superheat temperature increases gradually.

3. THERMAL NON EQUILIBRIUM MODEL

In this part of the study, a model has been created using the heat transfer module of Comsol Multiphysics. Values of radius of curvature (r_c), liquid thickness (δ_w) and temperature difference (ΔT) are obtained from the Matlab model. A 2D model is drawn first using these parameters and assigning boundary conditions, this model is solved for different values of the parameters for different values of angles to the liquid contact (θ). In this case, temperature difference is assigned to the bottom and upper boundaries attached to the liquid part of the model and all other boundaries are kept as thermally insulated boundaries. Using heat transfer in solid, material of solid is assigned as Copper and water for the liquid part from the Comsol Multiphysics material library. The thermal conductivity of water is manually assigned to 0.6 W/m-K. Using user defined refined mesh for the liquid part and basic triangular meshes for the solid part, the model is solved. Then in the postprocessing part, line integral is taken on the upper boundary of the liquid from the derived values. Line integral to the normal to the upper boundary of the liquid part gives us the value of heat flux at that particular boundary which represents how much heat per meter of length is being transferred from the boundary. For different values of angle to the liquid contact different values of heat flux per meter length is obtained. This result does not present the exact value of heat flux for which further modeling using surface model needs to be studied in 3D. This part is kept for the further study.

For 3 different values of l_p/d_p i.e. 1.2, 1.5 and 2 (as done in the Matlab model), heat flux is obtained to see how the trend looks like. From the result obtained from this study, it is found that the trend of the result follows nearly same path as obtained in Matlab model.

3.1 Modeling

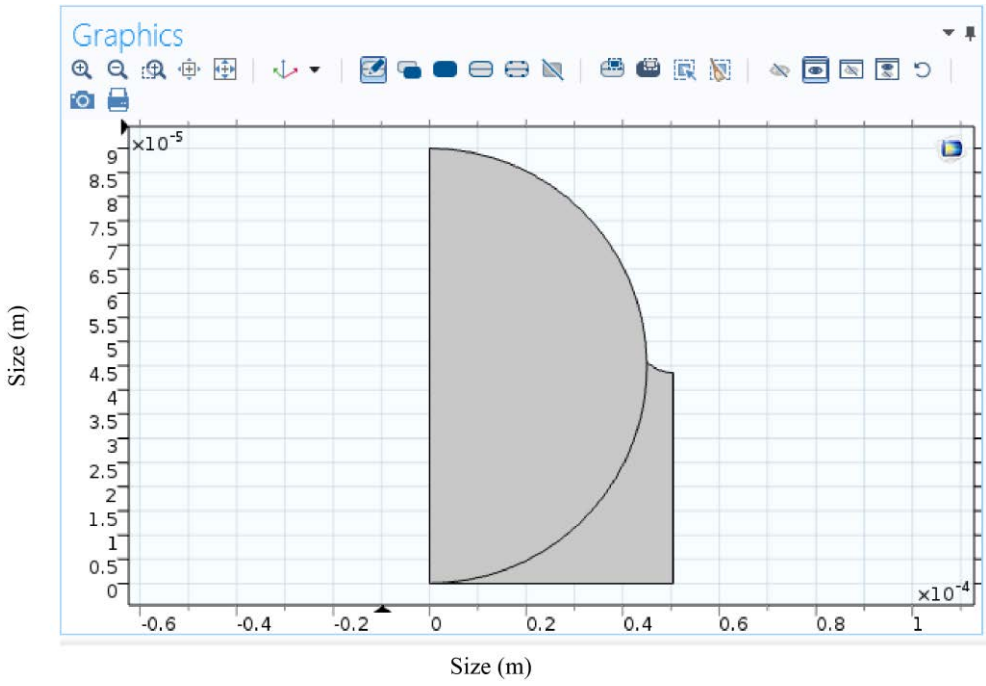

Figure 38 Geometry, drawn in Comsol Multiphysics

3.2 Boundary Conditions

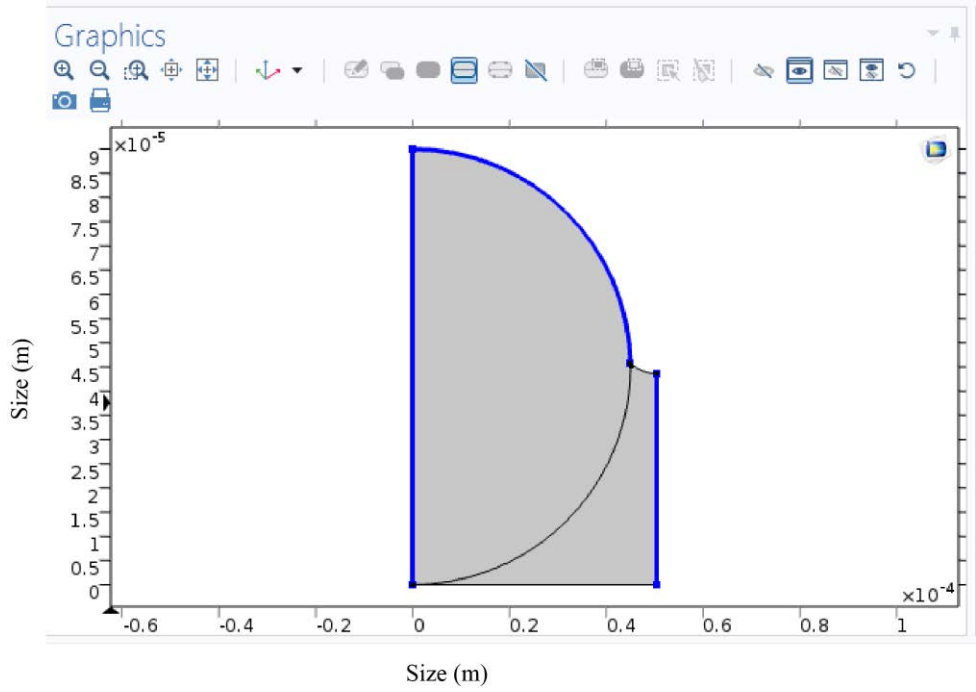

Figure 39 Insulation on the boundaries

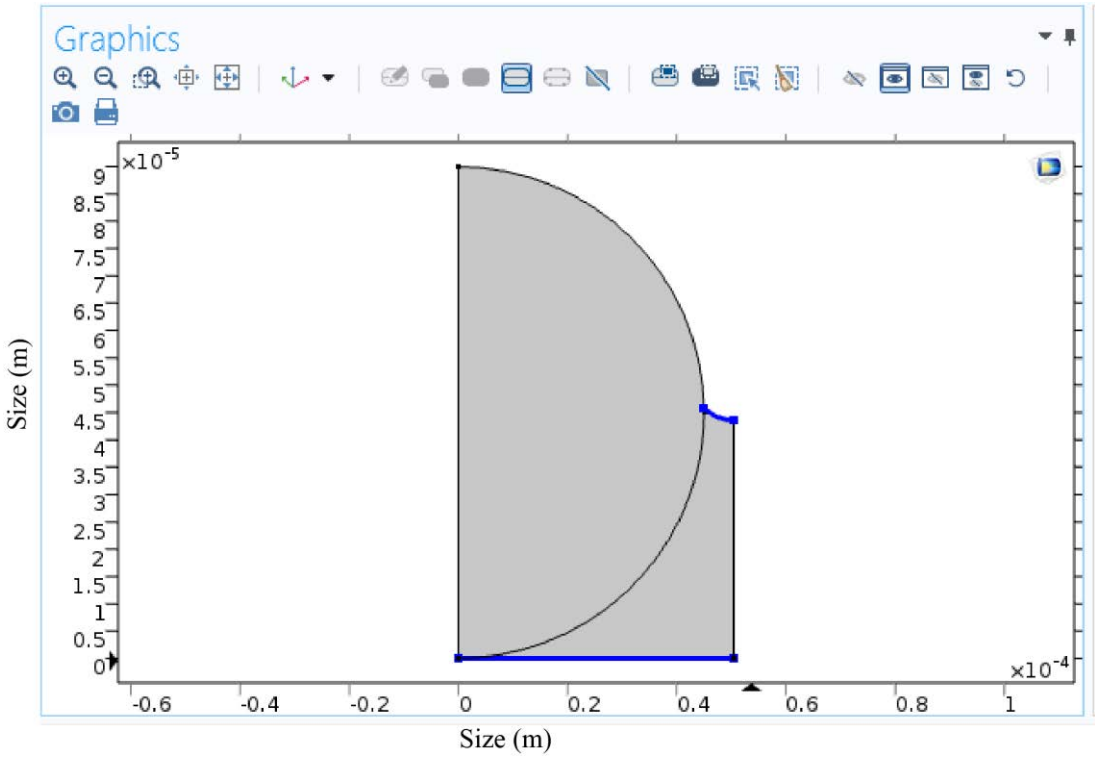

Figure 40 Temperature difference applied to these two boundaries

3.3 Meshing

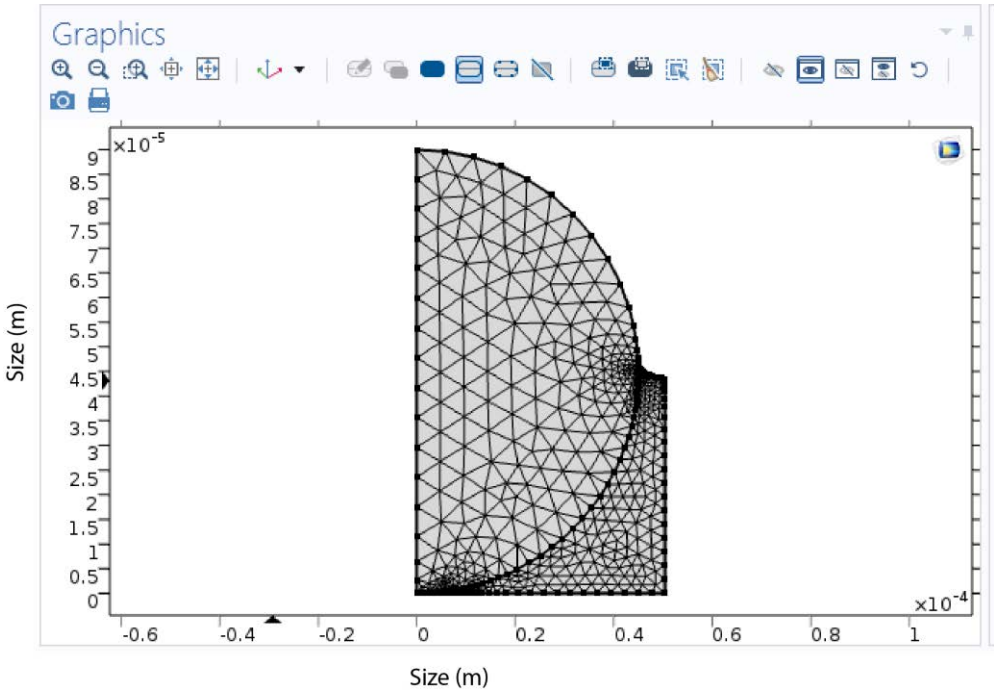

Figure 41 Mesh network of the model

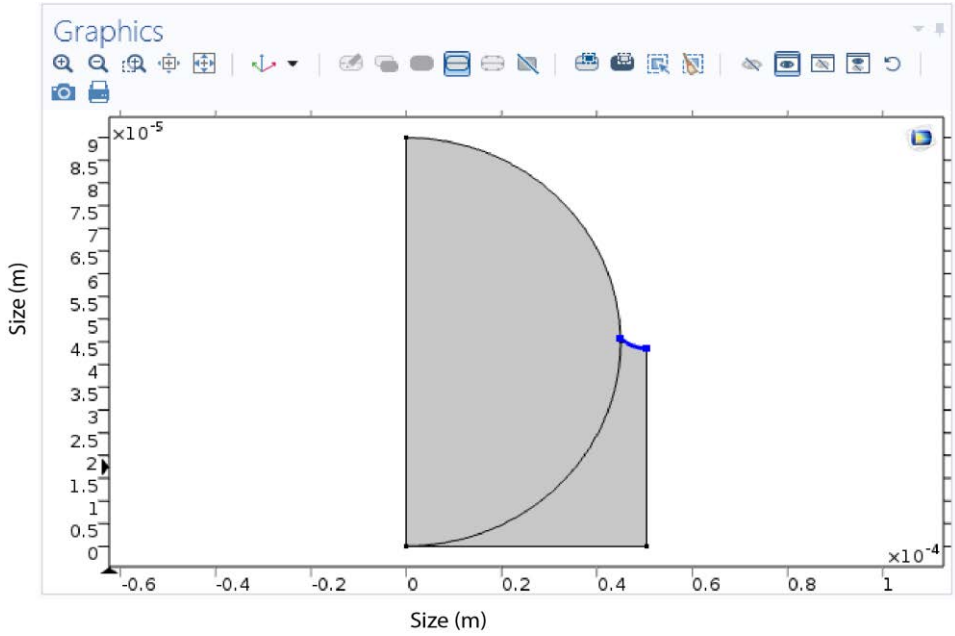

Figure 42 Heat flux calculation normal to the highlighted boundary (upper surface of the liquid)

3.4 Result

For l_p/d_p =1.12, and d_p =60μm, parameters obtained from Matlab for building up the model in Comsol Multiphysics along with the heat flux per unit length obtained from Comsol Multiphysics model are presented in the following table:

Table 4 For l_p/d_p =1.12, and d_p =60μm

Angle to the liquid contact θ	Radius of Curvature r_c (m)	Liquid Thickness δ_w(m)	Temperature Difference ΔT (K)	Heat Flux per unit length q (W/m)
46	6.8872e-4	5.0735e-5	0.876	59.616
60	2.9438e-5	4.3997e-5	16.451	1157
70	1.2799e-5	3.9061e-5	31.584	2227.3
80	7.0710e-6	3.3931e-5	45.956	3270.5
85	5.7782e-6	3.1263e-5	49.420	3498.2
87	5.4416e-6	3.0172e-5	49.594	3611.5

For l_p/d_p =1.5, d_p =60μm parameters obtained from Matlab for building up the model in Comsol Multiphysics along with the heat flux per unit length obtained from Comsol Multiphysics model are presented in the following table:

Table 5 For l_p/d_p =1.5, d_p =60μm

Angle to the liquid contact θ	Radius of Curvature r_c (m)	Liquid Thickness δ_w(m)	Temperature Difference ΔT (K)	Heat Flux per unit length q (W/m)
46	0.0013	5.0635e-5	2.8416	200.2
60	7.3485e-5	4.2496e-5	42.6753	3156.4
70	3.9774e-5	3.6534e-5	66.4286	4875.4
80	2.6946e-5	3.3036e-5	79.1150	5944.8
81	2.6148e-5	2.9699e-5	79.5343	5948.8
82	2.5410e-5	2.9059e-5	79.7808	6166.3

For l_p/d_p =2, d_p =60μm parameters obtained from Matlab for building up the model in Comsol Multiphysics along with the heat flux per unit length obtained from Comsol Multiphysics model are presented in the following table:

Table 6 For l_p/d_p =2, d_p =60μm

Angle to the liquid contact θ	Radius of Curvature r_c (m)	Liquid Thickness δ_w(m)	Temperature Difference ΔT (K)	Heat Flux per unit length q (W/m)
46	0.0022	5.0504e-5	3.4511	243.91
60	1.3144e-4	4.0521e-5	46.0856	3402.6
70	7.5267e-5	3.3209e-5	65.5008	4886.8
72	6.9315e-5	3.1716e-5	67.8056	4994.4
75	6.2044e-5	2.9452e-5	70.1294	5337.3
78	5.6286e-5	2.7157e-5	71.0214	5405.1

For every value of angle to the liquid contact, q(W/m) is plotted versus ΔT (K). A single line is found for each l_p/d_p value. From this graph we can conclude that the trend that is found from Matlab modeling matches with the one found from Comsol Multiphysics modeling.

As we already have l_p/d_p =1.12, and d_p=60μm result, to verify the particle diameter change effect, for l_p/d_p =1.12 and d_p=30μm and for l_p/d_p =1.12 and d_p=90μm results are required which are show in the following tables:

Table 7 For l_p/d_p =1.12, and d_p =30μm

Angle to the liquid contact θ	Radius of Curvature r_c (m)	Liquid Thickness δ_w(m)	Temperature Difference ΔT (K)	Heat Flux per unit length q (W/m)
46	3.4436e-4	2.5367e-5	0.2033	14.328
60	1.4719e-5	2.1998e-5	3.6362	265.6
70	6.3997e-5	1.9531e-5	6.6743	488.72
80	3.5355e-6	1.6965e-5	9.2356	672.56
83	3.1053e-6	1.6170e-5	9.5911	680.81
84	2.9908e-6	1.5901e-5	9.6430	697.65

Table 8 For l_p/d_p =1.12, and d_p =90μm

Angle to the liquid contact θ	Radius of Curvature r_c (m)	Liquid Thickness δ_w(m)	Temperature Difference ΔT (K)	Heat Flux per unit length q (W/m)
46	.0010	7.6102e-5	1.2955	89.12
60	4.4158e-5	6.5995e-5	25.4770	1861.00
70	1.9199e-5	5.8592e-5	50.5485	3729.00
80	1.0607e-5	5.0896e-5	76.5532	5450.00
85	8.6673e-6	4.6894e-5	84.2986	5966.70
89	7.7835e-6	4.3601e-5	85.3624	5967.00

3.5 Graphical presentation of the result

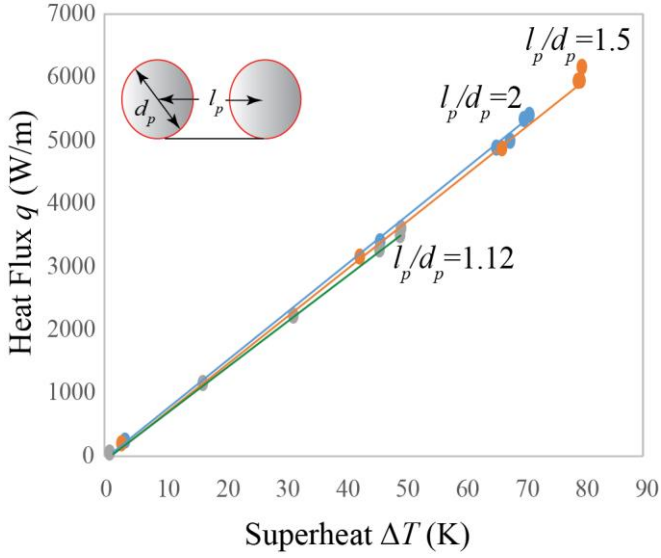

Figure 43 Heat flux q (W/m) versus superheat limit ΔT (K) for different distance between particles

Above figure shows how heat flux varies with distance between particles. If distance between two adjacent particles are too low, heat flux and temperature difference are both low.

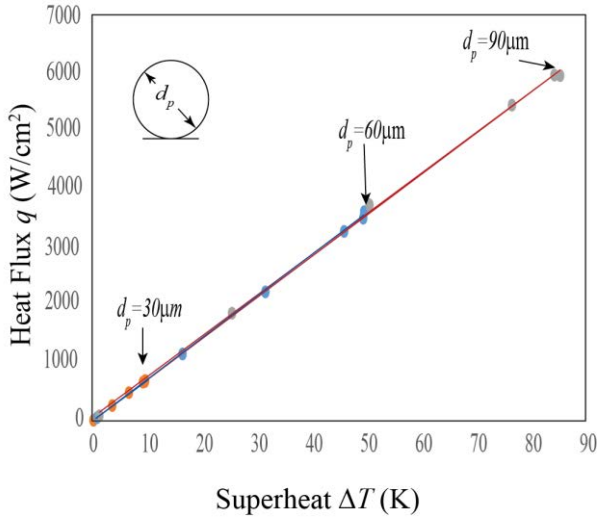

Figure 44 Heat flux q (W/m) versus superheat limit ΔT(K) for different particle diameters

With the increase in distance between adjacent particles, heat flux and temperature difference increases. But the temperature increase is such high that it is not feasible because of too much

penalty. Figure 44 represents how heat flux and temperature difference varies with the increase in particle diameter. If particle diameter is too low, heat flux and temperature difference both are low and if diameter is too high although heat flux is high but penalty due to high temperature difference is also high.

4. CONCLUSION

Heat flux in the monolayer (thin) wick with liquid artery wick is examined as a function of superheat using the elaborated, effective porosity, permeability, and liquid level aiming at designing the optimal capillary evaporator wick for high heat flux thermal management systems. Monolayer wick design dominantly controls CHF and thermal resistance, and optimal geometries are studied. It is found that if the value of porosity of the monolayer wick is low, it is favorable in both the heat flux and small wick superheat, when the relative permeability is proportional to liquid saturation. Large particle size is beneficial to the high heat flux at an expense of the thermal resistance. Also, the effective liquid traveling distance towards the evaporator site (number of columns) plays vital role to the performance of the system. This study provides a road map to optimally design monolayer wick for the heat flux and small thermal resistance based on microscale liquid morphologies near the evaporation sites.

From thermal equilibrium model, the main conclusions are the following.

- If the diameter of the particles is small (<30 μm), critical heat flux is small because permeability is low in the porous structure.
- If the diameter of the particles is high (>30μm) it leads to high permeability resulting in high CHF but superheat limit becomes high because amount of water contained in the micropore is high. So, ideal diameter should be from 50μm to 80 μm.
- If the distance between two particles is small, permeability is low which retards liquid supply resulting in low CHF. If the distance is high, liquid film thickness becomes too

low, as a result rapid dry-out occurs. So ideal distance should be from $1.12 \times d_p$ to 1.2 $\times d_p$.

- The performance is predicted using three relative permeability model and it is observed that $k_r = S$ agree with the experimental results. However future study will evaluate the exact permeability of monolayer wick.

From the non-equilibrium model, the following conclusions are drawn,

- If the distance between particles if small, heat transfer is low because, permeability is low.
- Optimal design of the distance between particles is in line with the results of Thermal Equilibrium model.
- Optimal particle distance is in range of 50μm-80μm

5. OUTLOOK AND FUTURE STUDIES

There are some suggestions about future studies,

I. By increasing the hydrophilic property of the micro particles, it is supposed to increase the heat transfer as the system is dominated by latent heat of evaporation. So, hydrophilic property test can be a further study.

II. Since the traveling distance is predominantly determined by the liquid artery wick, the geometrical optimization of liquid artery wick is further studied.

III. Using different particle size distributions, the performance may be studied.

IV. 2D model has limitations regarding heat transfer calculation so this study can be extended by including 3D non equilibrium model.

V. Model will be improved by using the combination of distances between particles.

REFERENCES

REFERENCES

[1] C.-C Yeh, C.-N Chen, Y.-M Chen, Heat transfer analysis of a loop heat pipe with biporous wicks, Int. J. Heat Mass Transfer 52 (2009) 4426-4434.

[2] T. Semenic, I. Catton, Experimental study of biporous wicks for high heat flux applications, Int. J. Heat Mass Transfer 52 (2009) 5113-5121.

[3] G.S. Hwang, Y. Nam, E. Fleming, P. Dussinger, Y.S. Ju, M. Kaviany, Multi-artery heat pipe spreader: Experiment, Int. J. Heat Mass Transfer 53 (2010) 2662-2669.

[4] D.H. Min, G.S Hwang, M. Kaviany Multi-artery, heat pipe spreader, Int. J. Heat Mass Transfer 52 (2009) 629-635.

[5] G.S. Hwang, E. Fleming, B. Carne, S. Sharratt, Y. Nam, P. Dussingger, Y.S. Ju, M. Kaviany, Multi-artery heat spreader: Lateral liquid supply, Int. J. Heat Mass Transfer 54 (2011) 2334-2340.

[6] G.P. Peterson, An Introduction to Heat Pipes: Modeling, Testing, and Applications, Wiley, New York, 1994.

[7] R. Ranjan, J. Y. Murthy, S. V. Garimella, A microscale model for thin-film evaporation in capillary wick structures, Int. J. Heat Mass Transfer 54 (2011) 169-179.

[8] K. K. Bodla, J. Y. Murthy, S. V. Garimella, Evaporation analysis in sintered wick microstructures, Int. J. Heat Mass Transfer 61 (2013) 729-741.

[9] G. S. Hwang, M. Kaviany, W. G. Anderson, J. Zuo, Modulated wick heat pipe, Int. J. Heat Mass Transfer 50 (2007) 1420-1434.

[11] K.K. Bodla, J. a Weibel, S. V Garimella, Advances in Fluid and Thermal Transport Property Analysis and Design of Sintered Porous Wick Microstructures, J. Heat Transfer. 135 (2013) 61202. doi:10.1115/1.4023569.

[12] Zuo, Z.J.; North, M.T.; Wert, K.L., "High heat flux heat pipe mechanism for cooling of electronics," Components and Packaging Technologies, IEEE Transactions on , vol.24, no.2, pp.220,225, Jun 2001 doi: 10.1109/6144.926386

[13] B &K Engineering, Inc. “Heat Pipe Design Handbook” volume 1. National Aeronautics and Space Flight Center Greenbelt, Maryland 20771.

[14] Gaugler, R.S. “Heat Transfer Devices”. US patent 2.350,348, June 6, 1944.

[15] Trefethen, L., "On the Surface Tension Pumping of Liquids or a Possible Role of the Candlewick in Space Exploration," G.E. Tech. Info., Serial No. 615 Dll4, February 1962.

APPENDIXES

A MATLAB PROGRAMS FOR THERMAL EQUILIBRIUM APPROACH

Matlab Program for Single Colum Temperature Distribution

```
Lh=1e-3; %Thickness of evaporator wall

Lhe=60e-6; %Thickness of evaporator wick

Lce=(1.93e-2+1.93e-2); %Thickness of condenser wick

Lc=1e-3; %Thickness of condenser wall



Kcu=401; %Thermal conductivity of copper

Ke=3.94; %Effective thermal conductivity

Kc=401;



Acu=(1e-2*1e-2); %Area of heater

Ae=8e-4; %Area of evaporator sperader

Ac=(12e-2*7e-2); %Area of condenser spreader

Aco=Ac; %Area if condenser



Rh=(1/(Lh/(Kcu*Acu))) %Thermal resistance of heater

Rhe=(1/(Lhe/(Ke*Ae))) %Thermal resistance of evaporator wick

Rce=(1/(Lce/(Kc*Ac))) %Thermal resistance of condenser wick

Rc=(1/(Lc/(Kc*Aco))) %Thermal resistance of condenser
```

```
a=-5;

T1=55+273;

for i=1:4

T1=T1+a %Temperature of heater

T5=30+273; %Temperature of condenser




P=[(-Rh-Rhe) Rhe 0; Rhe (-Rhe-Rce) Rce; 0 Rce (-Rce-Rc)];

Q=[-T1*Rh; 0; -T5*Rc];



T=inv(P)*Q

end
```

Matlab Program for Single Column Pressure Distribution

```
Q = 31.06; % Energy, W

hlg= 2260000; % latent heat of evaporation, j/kg

p4= 101325; %condenser pressure at point 4, pa

rho= 1000; % density 1000 kg/m^3

K= 2.15168e-12; %permeability m^2
```

```
u= 0.001; %viscosity Ns/m^2

A1= 4e-2*60e-6; %evaporator cross sectional area

A2= pi*(3e-3)^2/4; %liquid column cross sectional area

A3= (12e-2+7e-2)*2e-2; %condenser cross sectional area

l1=1e-3; %length considered for flow in evaporator

l2=1e-2; %length of liquid column

l3=1e-3; %length considered for flow in condenser

R1=((u*l1)/(rho*A1*k)); %resistance in evaporator

R2=((u*l2)/(rho*A2*k)); %resistance in liquid column

R3=((u*l3)/(rho*A3*k)); %resistance in cofdndenser

B= [(1/R1) -((1/R1)+(1/R2)) (1/R2);0 (1/R2) -((1/R2)+(1/R3));0 0 (1/R3)];

C=[0;-(p4/R3);((p4/R3)-(Q/hlg))];

P=inv(B)*C

S=71.97e-3; % S= Surface tension
```

```
rc=0.41*0.5*60e-6;

Cr=2*S/rc %Limiting Criterion
```

Matlab Program for Diameter Change and Distance Between Particles

```
x=101*pi/180; %theta

xc=45*pi/180; %theta C



%Q = 105.8323; % Energy, W

hlg= 2260000; % latent heat of evaporation, j/kg

p4= 101325; %condenser pressure at point 4, pa

rho= 1000; % density 1000 kg/m^3

%k= 2.15168e-12; %permeability m^2

u= 0.001; %viscosity Ns/m^2



A1= 4e-2*60e-6; %evaporator cross sectional area

A2= pi*(3e-3)^2/4; %liquid column cross sectional area

A3= (12e-2+7e-2)*2e-2; %condenser cross sectional area



l1=1e-3; %length considered for flow in evaporator

l2=1e-2; %length of liquid column

l3=1e-3; %length considered for flow in condenser
```

```
dp=zeros(35,1);

lp=zeros(35,1);

rc=zeros(35,1);

dw=zeros(35,1);

E=zeros(35,1);

k=zeros(35,1);

R1=zeros(35,1);

R2=zeros(35,1);

R3=zeros(35,1);

B=zeros(35,1);

C=zeros(35,1);




Lh=1e-3; %Thickness of evaporator wall

Lhe=60e-6; %Thickness of evaporator wick

Lce=(1.93e-2+1.93e-2); %Thickness of condenser wick

Lc=1e-3; %Thickness of condenser wall



Kcu=401; %Thermal conductivity of copper
```

```
Ke=3.94; %Effective thermal conductivity

Kc=401;



Acu=(1e-2*1e-2); %Area of heater

Ae=1e-4; %Area of evaporator sperader

Ac=(12e-2*7e-2); %Area of condenser spreader

Aco=Ac; %Area if condenser



Rh=(1/(Lh/(Kcu*Acu)));  %Thermal resistance of heater

Rhe=(1/(Lhe/(Ke*Ae)));  %Thermal resistance of evaporator wick

Rce=(1/(Lce/(Kc*Ac)));  %Thermal resistance of condenser wick

Rc=(1/(Lc/(Kc*Aco))) ;  %Thermal resistance of condenser



T1=50+273;  %Temperature of heater

R=[(-Rh-Rhe) Rhe 0; Rhe (-Rhe-Rce) Rce; 0 Rce (-Rce-Rc)];

%hold on;

for i=1:10

    %hold on;

   figure (i);
```

```
    for j=1:15
        T5=34+273+j;
        Z=[-T1*Rh; 0; -T5*Rc];
        T=R\Z;
        Q=(T1-T(1,1))*Rh;

dp(i)=34e-6+i*10^-6; %diameter of particle
lp(i)=1.12*dp(i); %space between two particles

rc(i)=(2/3^0.5*lp(i)-dp(i)*sin(x))/(2*sin(x-xc)); %meniscus radius
dw(i)=0.5*(dp(i)*(1+cos(x))-rc(i)*(1-cos(x-xc))); %fluid layer thickness
E(i)=1-(2*pi/(3^0.5*lp(i)^2*dw(i)))*((2/3*(dp(i)/2)^3)+(dp(i)/2)^2*(dw(i)-(dp(i)/2))-
(1/3)*(dw(i)-dp(i)/2)^3); %porosity
k(i)=(dw(i)/dp(i))*(E(i)^3*dp(i)^2/(180*(1-E(i))^2)); %permeability

R1(i)=((u*l1)/(rho*A1*k(i))); %resistance in evaporator
R2(i)=((u*l2)/(rho*A2*k(i))); %resistance in liquid column
R3(i)=((u*l3)/(rho*A3*k(i))); %resistance in cofdndenser
```

```
B= [(1/R1(i)) -((1/R1(i))+(1/R2(i))) (1/R2(i));0 (1/R2(i)) -((1/R2(i))+(1/R3(i)));0 0
(1/R3(i))];

C=[0;-(p4/R3(i));((p4/R3(i))-(Q/hlg))];


P=B\C;


S=71.97e-3; % S= Surface tension

rc=0.41*0.5*60e-6;

Cr=2*S/rc; %Limiting Criterion

dP=101325-P(1,1);

 %hold on;

if dP<Cr

    T;

    Q

    dT=T1-T5

    dia=dp(i,1)

    Cr;

    dP;

    hold on;

    plot(dT,Q,'--ro');
```

```
    xlabel('Temperature Difference dT oC');

    ylabel('Heat flux (W/cm^2)');

end

    end

end
```

Matlab Program for Finding Design Parameters and Monolayer with Liquid Artery Heat Flux

```
clear all;

clc;

dp=90e-6; %particle diameter

lp=1.12*dp; %distance between particles

hlg=2260000; %latent heat of evaporation

xc=45*pi/180; %angle to the liquid contact

u=0.001; %viscosity

rho= 1000; % density 1000 kg/m^3

l1=0.25*3.2e-3;

l2=1e-3;

l3=0.25*3.2e-3;

p4=101325;
```

```
% a1=0;
% b1=0;
%
  for i=1:85
    x=(45+i)*pi/180; %Contact angle

    rc=((lp-dp*sin(x))/(2*sin(x-xc))); %radius of curvature
    dw=(dp/2)*(1+cos(x))-rc*(1-cos(x-xc)); %liquid thickness
    v=(asin((1/rc)*(dp/2-lp/2)));
    A=(rc+dw)*((lp/2-((dp/2))))+(rc^2/2)*v+(rc^2/4)*sin(2*v);
    y=dp/2+dp/2*cos(x);
    vw=2*(A*lp)+4*(A*dp/2)+dp^2/4*(y)-(1/4)*(pi*(y^2*(dp/2)-(y^3/3)));%volume
occupied by water only
    vp=dp*lp^2-(1/6)*pi*dp^3; %pore volume
    S=vw/vp;
    e=1-(1/6)*pi*(dp/lp)^2; %porosity

    Ke=0.66*(401/.66)^(0.28-0.757*log(e)-0.057*log(401/.66)); %Effective thermal
conductivity
```

```
K=((e^3*dp^2)/(180*(1-e)^2)); %permeability

Kr=K;%relative permeability


A1=4*dw*1e-2;

A2=4*lp*lp;

A3=4*dw*1e-2;


R1=((u*l1)/(rho*A1*Kr)); %resistance in evaporator

R2=((u*l2)/(rho*A2*Kr)); %resistance in liquid column

R3=((u*l3)/(rho*A3*Kr)); %resistance in cofdndenser



Si=71.97e-3; % Si= Surface tension

Cr=(2*Si*cos(xc))/rc; %Limiting Criterion


m1=Cr*(rho/u)/(((0.25*3.2e-3)/(4*dw*1e-2*Kr))+(1e-2/(9.089e-11*7.069e-6))+((3.2e-
3)/(2.52e-10*4*1e-2*7.581e-5))); % mass flow rate

Q=m1*hlg;

dP=m1*R1;
```

```
%     Q=m1*hlg %heat transfered
%     %B= [(1/R1) -((1/R1)+(1/R2)) (1/R2);0 (1/R2) -((1/R2)+(1/R3))0; 0 (1/R3(i))];
%     B= [(1/R1) -((1/R1)+(1/R2)) (1/R2);0 (1/R2) -((1/R2)+(1/R3));0 0 (1/R3)];
%     C=[0;-(p4/R3);((p4/R3)-(Q/hlg))];
%
%     P=B\C
    dT=Q*dw/(1e-4*Ke); %Temperaturemdifference
%     p1=101325*((1/R1)+(1/R2))*R1;
%     dP= 101325-p1
%     if dP>Cr
%         break;
%     else
        x*180/pi;
        rc;
    dw;
    Q;
    dT;
    dP;
    R=dw/(1e-4*Ke);
       hold on;
```

```
        plot (x*180/pi,e,'*r');


%
%     end
%    end
%    a1=Q;
%    b1=dT;
%
%    hold on;
%    plot(dT,Q,'*r')
%    xlabel('Temperature Difference \Delta T {\circ}C');
%    ylabel('Critical Heat Flux q_{CHF} W/cm^2');
%    m(i)= Q;
%    n(i)=dT;
%    w(i)=m1;
%   if dw<0
%       break
%   end
  end
 e;
```

K;

Ke

B COMSOL MODELING FOR THERMAL NON-EQUILIBRIUM APPROACH

Comsol Stepwise Simulation Report

Date

Apr 23, 2015 6:36:51 PM

Contents

Global

Used products
COMSOL Multiphysics

Component

Definitions

Coordinate Systems

Boundary System

Coordinate system type	Boundary system
Tag	sys1

Geometry

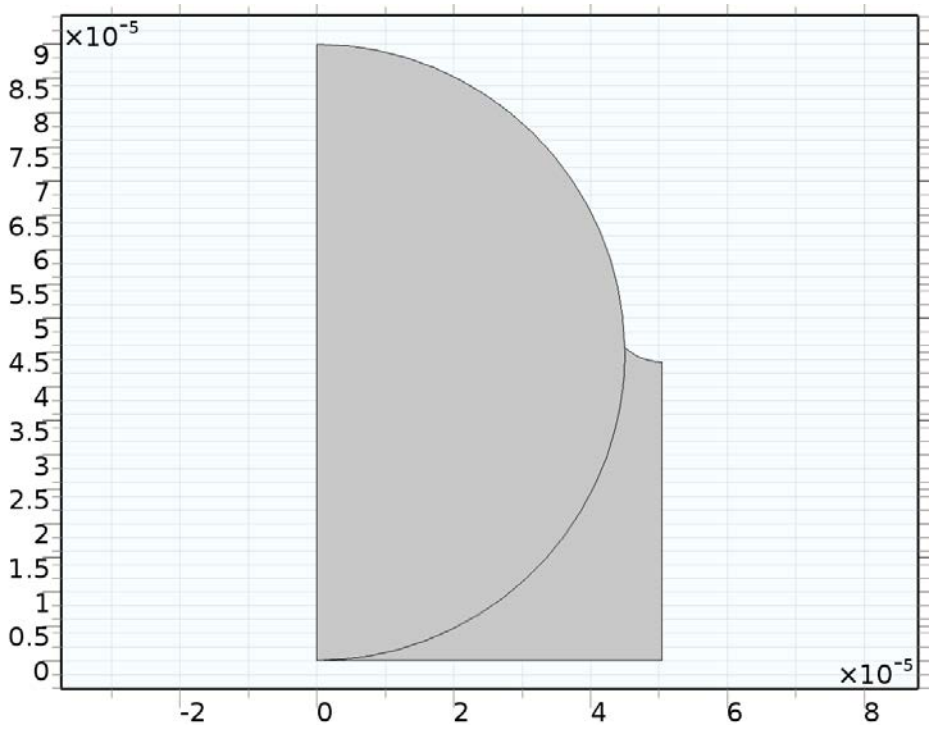

Geometry

Units	
Length unit	m
Angular unit	deg

Materials

Copper

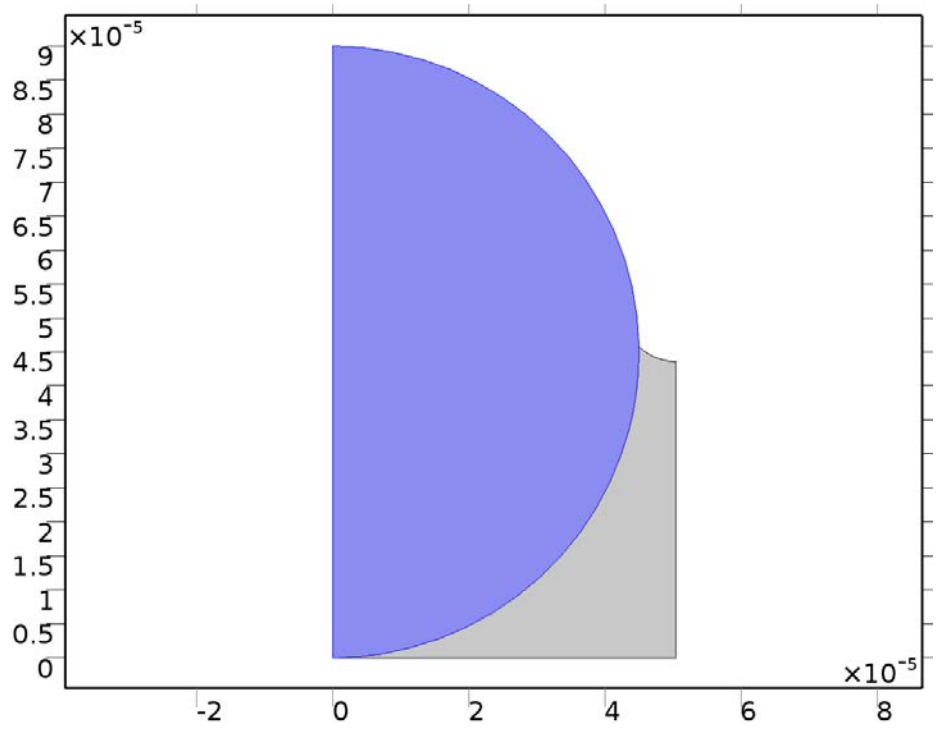

Copper

Selection	
Geometric entity level	Domain
Selection	Domain 1

Water, Liquid

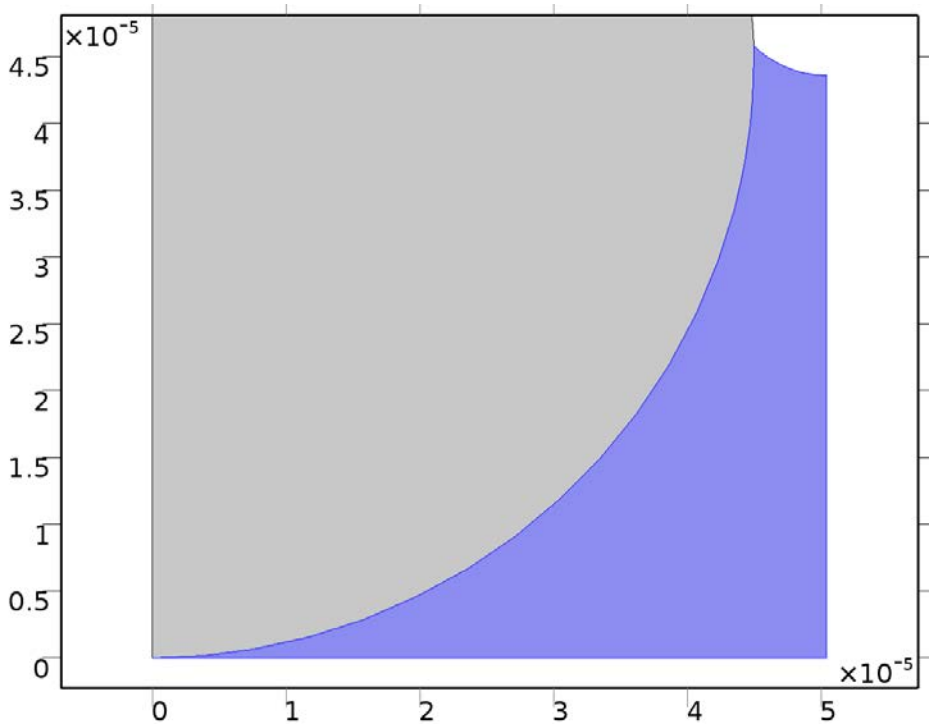

Water, liquid

Selection	
Geometric entity level	Domain
Selection	Domain 2

Heat Transfer in Solids

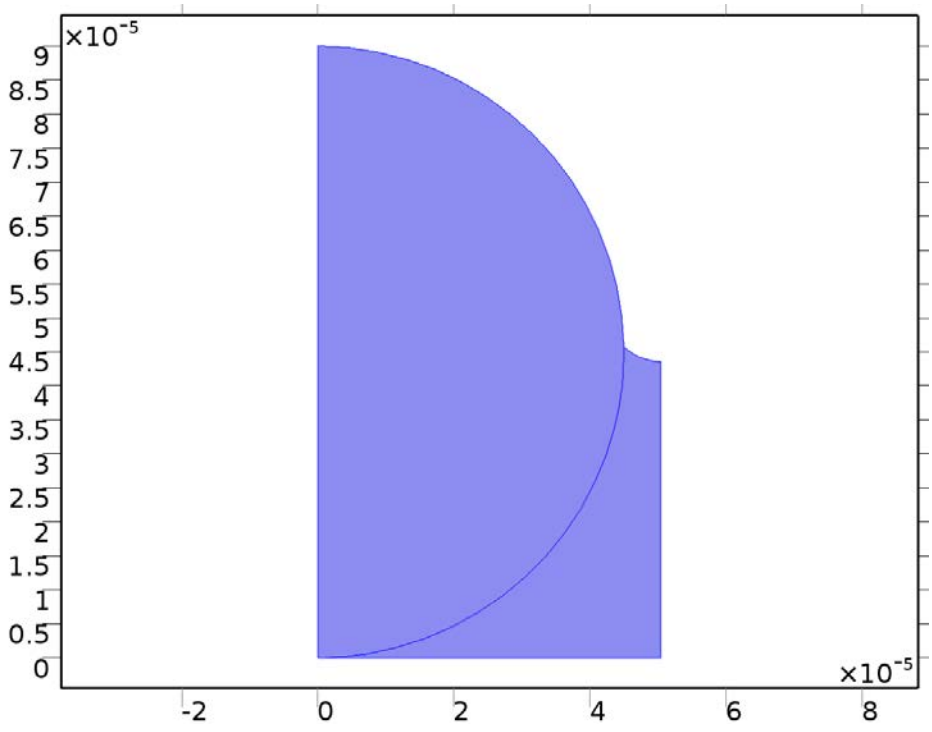

Heat Transfer in Solids

Features
Heat Transfer in Solids 1
Initial Values 1
Thermal Insulation 1
Heat Transfer in Fluids 1
Temperature 1
Temperature 2

Mesh

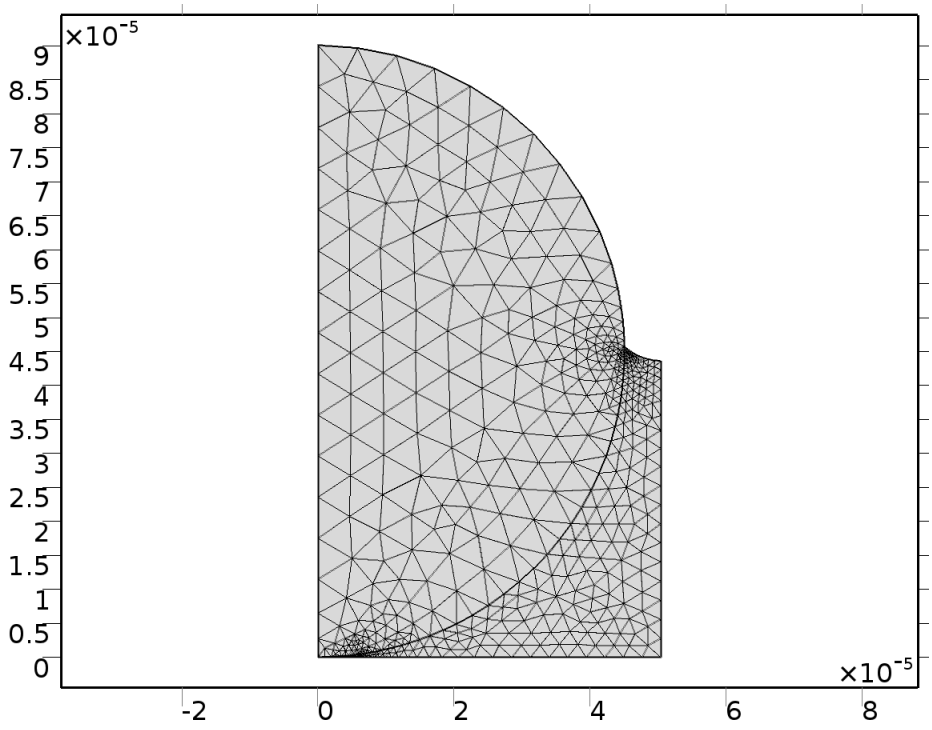

Mesh 1

Study

Stationary

Study settings	
Property	**Value**
Include geometric nonlinearity	Off

Physics and variables selection	
Physics interface	**Discretization**
Heat Transfer in Solids (ht)	physics

Mesh selection	
Geometry	**Mesh**
Geometry 1 (geom1)	mesh1

Results

Data Sets

Study 1/Solution 1

Solution	
Name	**Value**
Solution	Solution 1
Component	Save Point Geometry 1

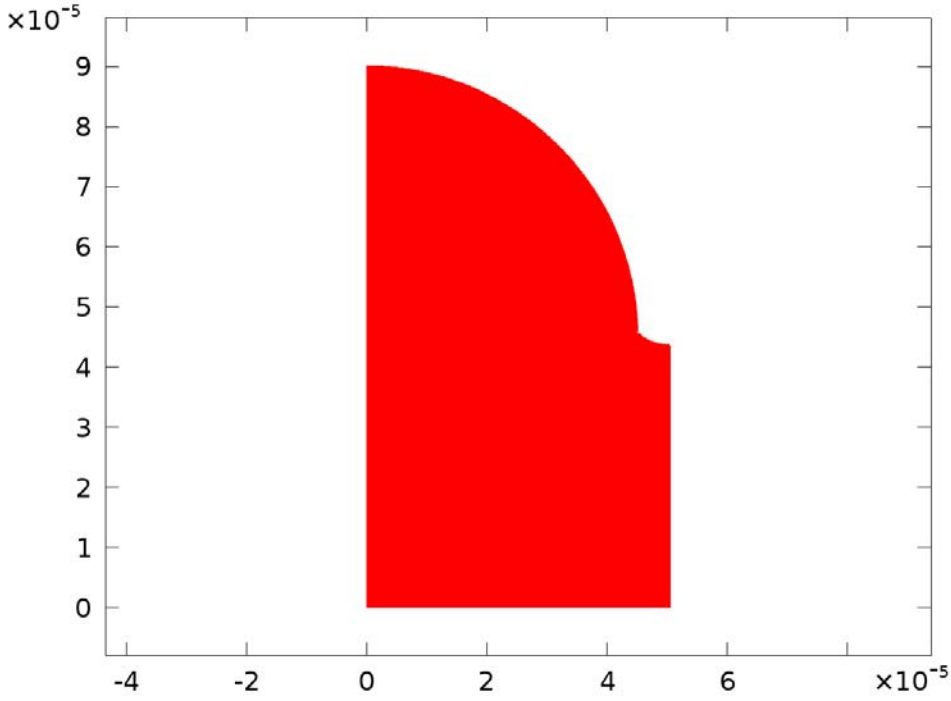

Data set: Study 1/Solution 1

Cut Line 2D 1

Data	
Name	**Value**
Data set	Study 1/Solution 1

Line data	
Name	**Value**
Line entry method	Two points
Points	{{-2.29057E-6, 1.04906E-5}, {3.32E-5, 9.86792E-6}}

Advanced	
Name	**Value**
Space variable	cln1x

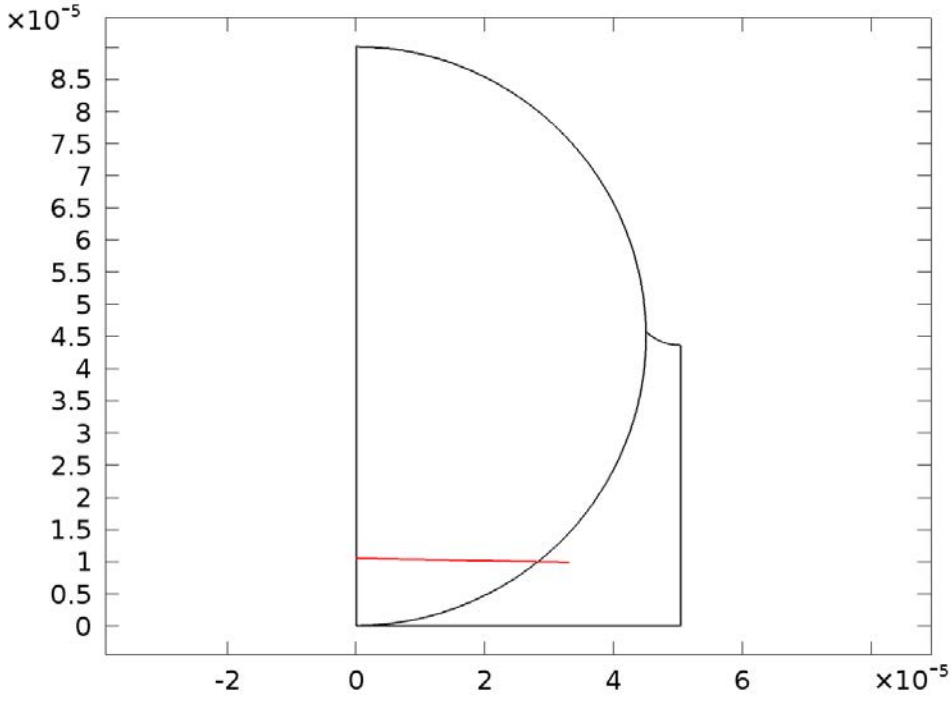

Data set: Cut Line 2D 1

Cut Line 2D 2

Data	
Name	**Value**
Data set	Study 1/Solution 1

Line data	
Name	**Value**
Line entry method	Two points
Points	{{-2.91321E-6, 2.59528E-5}, {3.69358E-5, 2.59528E-5}}

Advanced	
Name	**Value**

Space variable	cln2x

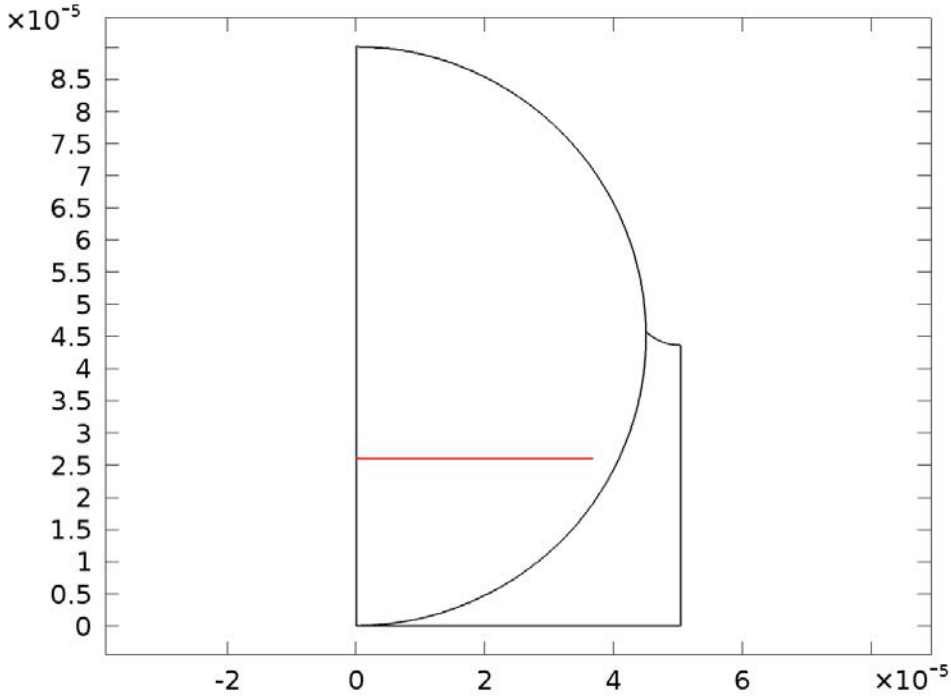

Data set: Cut Line 2D 2

Cut Line 2D 3

Data	
Name	**Value**
Data set	Study 1/Solution 1

Line data	
Name	**Value**
Line entry method	Two points
Points	{{-2.54793E-7, 1.05934E-7}, {3.35751E-5, 1.05934E-7}}

Advanced	
Name	**Value**
Space variable	cln3x

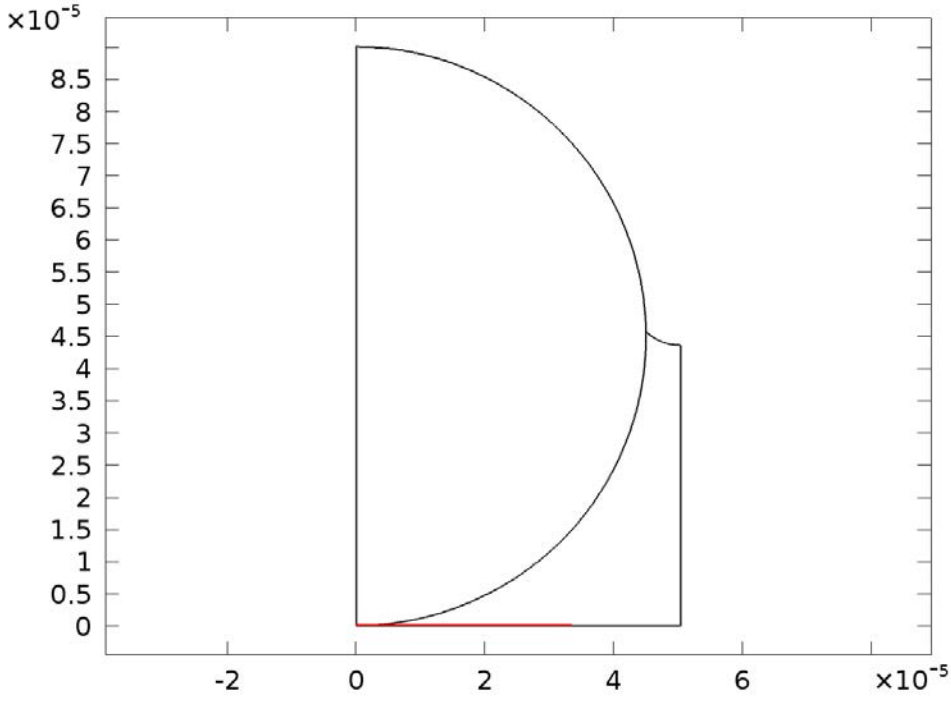

Data set: Cut Line 2D 3

Derived Values

Surface Integration 1

Selection	
Geometric entity level	Domain
Selection	Domains 1–2

Data	
Name	**Value**
Data set	Study 1/Solution 1

Expression	
Name	**Value**
Expression	ht.tfluxy
Unit	W
Description	Total heat flux, y component

Line Integration 2

Selection	
Geometric entity level	Boundary
Selection	Boundary 7

Data	
Name	**Value**
Data set	Study 1/Solution 1

Expression	
Name	**Value**
Expression	ht.ntflux
Unit	W/m
Description	Normal total heat flux

Line Average 1

Selection	
Geometric entity level	Boundary
Selection	Boundary 7

Data	
Name	**Value**
Data set	Study 1/Solution 1

Expression	
Name	**Value**
Expression	ht.ny
Unit	1
Description	Normal vector, y component

Tables

Table 1

Surface Integration 1 (ht.tfluxy)

Table 1			
Total heat flux, y component (W)	**Total heat flux, y component (W)**	**Total heat flux, y component (W)**	**Normal total heat flux (W/m)**
0.0000	0.0000	0.015782	72.461

Table 2

Line Maximum 1 (ht.ntflux)

Table 2						
Normal total heat flux (W/m^2)	**Normal total heat flux (W/m^2)**	**Normal total heat flux (W/m^2)**	**Normal total energy flux (W/m^2)**	**Normal total energy flux (W/m^2)**	**Normal total energy flux (W/m^2)**	**Normal total energy flux (W/m^2)**
0.0000	-1.5215E5	8.2344E8	8.2344E8	-1.5215E5	8.2344E8	3.6482E-5

Table 3

Surface Integration 1 (T)

Table 3
Total heat flux, y component (W)
0.035047

Table 4

Line Maximum 1 (ht.ntflux)

Table 4

Normal total heat flux (W/m^2)	Normal total heat flux (W/m^2)	Normal total heat flux (W/m^2)	Normal total heat flux (W/m^2)	Normal total heat flux (W/m^2)
-1.5215E5	9.3677E-5	8.2344E8	3.6482E-5	-1.5215E5

Table 5

Line Integration 2 (ht.ntflux)

Table 5					
Normal total heat flux (W/m)	**Normal total heat flux (W/m)**	**Normal total heat flux (W/m)**	**Normal total heat flux (W/m)**	**Normal total heat flux (W/m)**	**Normal total heat flux (W/m)**
-351.18	-343.26	343.26	327.73	327.73	327.73

Evaluation 2D

Interactive 2D values

Evaluation 2D		
x	**y**	**Value**
2.9744E-5	4.3823E-5	330.27

Table 6

Line Average 1 (T)

Table 6
Normal vector, y component (1)
0.92314

Table 7

Line Integration 2 (ht.ntflux)

Table 7

Normal total heat flux (W/m)
327.73

Table 8

Line Integration 2 (ht.ntflux)

Table 8			
Normal total heat flux (W/m)	**Normal total heat flux (W/m)**	**Normal total heat flux (W/m)**	**Normal total heat flux (W/m)**
655.87	655.87	65.512	70.221

Plot Groups

Temperature (Ht)

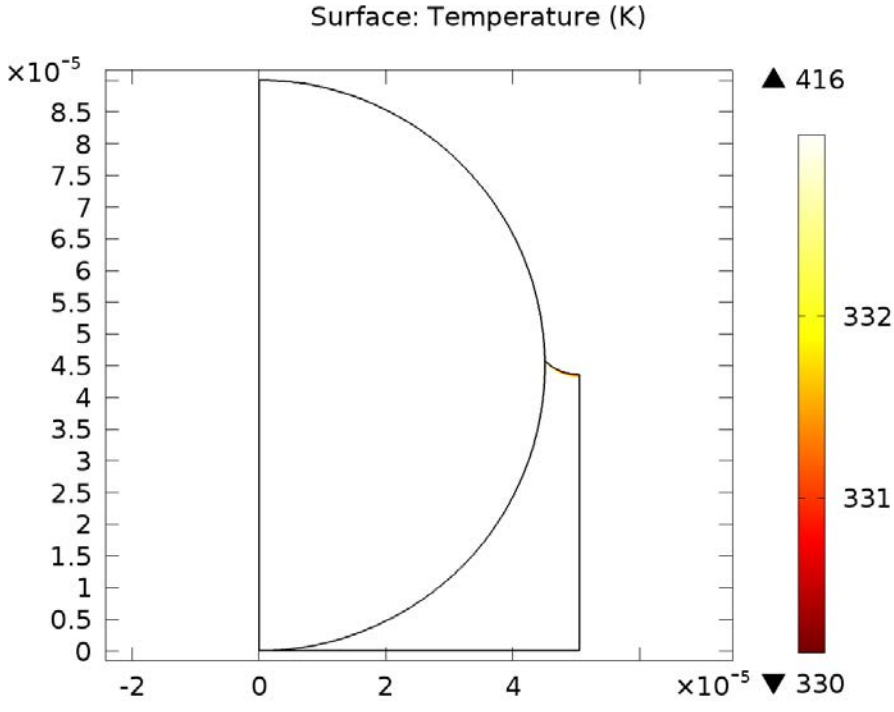

Surface: Temperature (K)

Isothermal Contours (Ht)

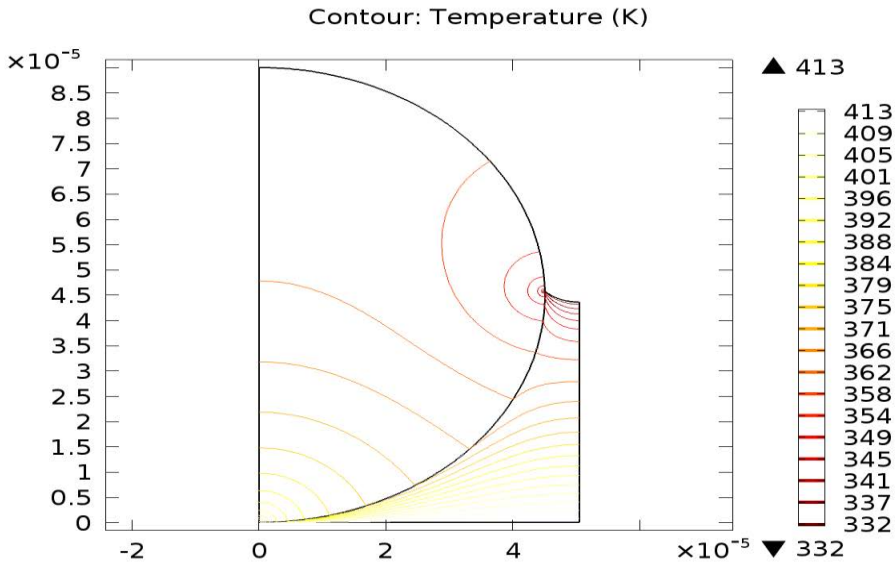

Contour: Temperature (K)

2D Plot Group 3

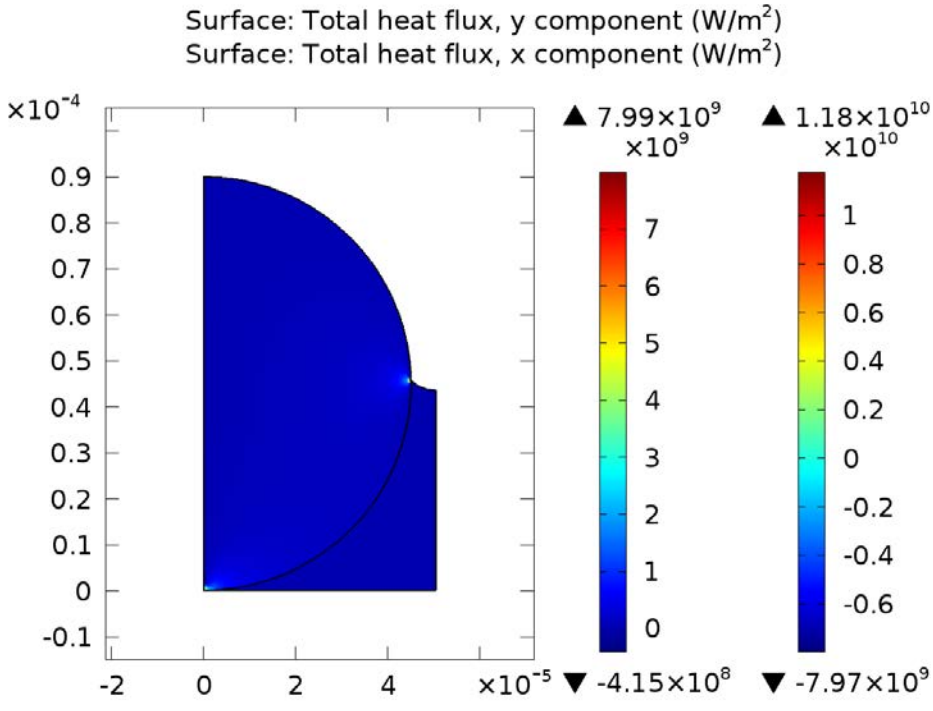

Surface: Total heat flux, y component (W/m2) Surface: Total heat flux, x component (W/m2)

1D Plot Group 4

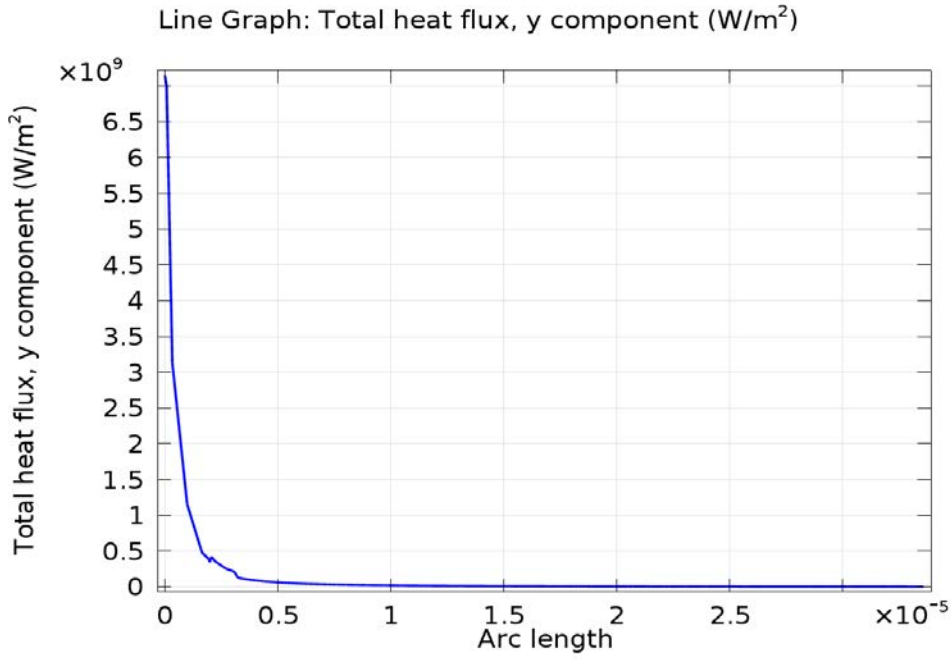

Line Graph: Total heat flux, y component (W/m2)